CORA Cork Open Research Archive
Cartlann Taighde Oscailte Chorcaí

Title	Energy variability and tilt angle in hybrid offshore wind – solar PV farms
Authors	Moore, Josh;Iglesias, Gregorio
Publication date	2026-09-11
Original Citation	Moore, J & Iglesias, G 2026, 'Energy variability and tilt angle in hybrid offshore wind – solar PV farms', Energy Conversion and Management: X, vol. 32, 102286, pp. 1-20. https://doi.org/10.1016/j.ecmx.2026.102286
Type of publication	Article (peer-reviewed)
Link to publisher's version	https://www.scopus.com/pages/publications/105051040476 - 10.1016/j.ecmx.2026.102286https://linkinghub.elsevier.com/retrieve/pii/S2590174526007695
Rights	© 2026, the Authors. Published by Elsevier Ltd. This is an open access article under the CC BY license (http://creativecommons.org/licenses/by/4.0/) - https://creativecommons.org/licenses/by/4.0/
Download date	2026-11-17 06:33:49
Item downloaded from	https://hdl.handle.net/10468/19315



UCC
University College Cork, Ireland
Coláiste na hOllscoile Corcaigh

Energy Conversion and Management: X 32 (2026) 102286

Contents lists available at ScienceDirect

Energy Conversion and Management: X

journal homepage: www.sciencedirect.com/journal/energy-conversion-and-management-x

Energy variability and tilt angle in hybrid offshore wind – solar PV farms

Josh Moore [a], Gregorio Iglesias [b,c,*]

[a] School of Engineering & Architecture, University College Cork, College Road, Cork, Ireland
[b] School of Engineering & Architecture & MaREI, Environmental Research Institute, University College Cork, College Road, Cork, Ireland
[c] School of Engineering, Computing and Mathematics, Drake Circus, Plymouth PL4 8AA, UK

ARTICLE INFO

Keywords:
Offshore renewable energy
Hybrid farm
Wind – solar
Angle of tilt
Energy variability
Balancing costs

ABSTRACT

Hybrid offshore renewable energy systems have great potential for realising infrastructure, operations and maintenance, and economic synergies – not least the smoothing of the variability of the energy output, which reduces the balancing costs. The focus of this work is the hybridisation of existing offshore wind farms with floating solar photovoltaic energy and, more specifically, the effects of the tilt angle of the solar photovoltaic installation on this variability, which have not been investigated so far. Two operational offshore wind farms, Westermost Rough (United Kingdom) and South Fork (United States), are selected as case studies. The analysis is conducted across three temporal resolutions: hourly, daily, and monthly. The variability of the energy output is analysed across 121 different tilt angles, ranging from 0 to 60 degrees in 0.5-degree increments. The following key results are obtained: (i) on an hourly timescale, the optimal tilt angle is 0°, though this results in a lower energy yield; (ii) on a daily timescale, the optimal tilt angle was below the magnitude of the latitude of Westermost Rough and South Fork, respectively; (iii) on a monthly timescale, the optimal tilt angles were also lower than the latitude of the two sites, respectively; and (iv) across all timescales, the level of energy output smoothing for different tilt angles has a notable impact on the overall capacity factor of the hybrid offshore wind-solar farm. Importantly, for any tilt angle, the hybridisation of the offshore wind farms through a floating solar photovoltaic system significantly smoothed the energy output.

1. Introduction

Electricity reliability is becoming an increasingly significant concern as renewable electricity generation expands globally to mitigate anthropogenic global warming. The reliability of the electricity supply is essential for a thriving economy and society, as it plays a key role in supporting economic productivity and societal well-being [1]. For this reason, and with the aim of reducing the variability of the energy supply, system operators worldwide have pushed to diversify renewable energy sources both spatially and technologically to reduce the variability of the energy supply.

Offshore renewable energy is key to decarbonising the energy system, and its potential is being realised rapidly. In particular, the offshore wind industry has seen remarkable growth, with 10.8 GW of global capacity installed in 2023 and 8.8 GW of capacity installed in 2022, bringing the total installed offshore capacity globally to 75.2 GW at the end of 2023 [2,3]. The capital investment needed for offshore wind projects is substantial compared with onshore projects [4]. However, offshore wind offers significant advantages, including increased space for larger turbines with wider spacing, diminished visual and noise impacts, and last, but not least, higher and less variable wind speeds due to the lower surface roughness of the ocean [5–8].

Integrating multiple renewable energy technologies in the same offshore farm offers key benefits for increasing the reliability of supply [9]. Among the options available, hybrid offshore wind-solar farms stand out [10]; they capitalise on the complementarity of wind and solar resources, i.e., on their low and, sometimes even negative [11], correlation. This concept has been extensively examined in the literature, including studies by Costoya et al. [12], Huang and Iglesias [10], de Souza Nascimento et al. [13] and Martinez and Iglesias [11]. Another interesting option is the hybridisation of offshore wind with wave energy, which has been investigated by, e.g., Pérez-Collazo et al. [14], Astariz and Iglesias [15] and Gaughan and Fitzgerald [16].

However, there has been increasing interest in offshore hybrid wind-solar farms due to the stronger complementarity between wind and solar resources compared to wind and wave energy [11,15], as well as the demonstrated successes of hybrid onshore projects such as the Port Augusta Renewable Energy Park in southern Australia [17]. This

* Corresponding author at: MaREI, Environmental Research Institute & School of Engineering, College Road, Cork, P43 C573, Ireland.
E-mail address: gregorio.iglesias@ucc.ie (G. Iglesias).

https://doi.org/10.1016/j.ecmx.2026.102286
Received 12 June 2025; Received in revised form 31 March 2026; Accepted 4 September 2026
Available online 11 September 2026
2590-1745/© 2026 The Authors. Published by Elsevier Ltd. This is an open access article under the CC BY license (http://creativecommons.org/licenses/by/4.0/).

complementary may be expected to reduce variability and, consequently, balancing costs – the additional expenses incurred in maintaining system stability due to the variability of wind energy. More specifically, wind energy is generally traded in day-ahead markets, where the power producer trades the forecasted energy generation for the next day. Due to complex nature of forecasting wind, grid operators must use balancing reserves, which are typically more expensive than energy traded in day-ahead markets, to compensate for any shortfall in anticipated generation [18]. Ultimately, these costs are typically borne by electricity consumers rather than the power producers themselves. Worryingly, these costs are expected to increase as wind penetration increases [19].

For its part, solar photovoltaic (PV) has a lower forecasting error compared to wind [20]. This, together with the low or, in some cases, even negative correlation between solar and wind energy resources, renders it attractive for the purposes of hybridisation and, in particular, for reducing the uncertainty of the overall energy production of the hybrid farm.

In addition, deploying floating solar PV (FPV) alongside offshore wind offers valuable synergies. First, hybridising offshore wind farms with floating solar PV (FPV) systems significantly boosts the overall energy yield of the site. Offshore wind farms occupy vast swathes of ocean. The wide spacing between turbines provides ample room for FPV deployment, enabling the installation of substantial solar capacities. For example, [21] found that the annual energy yield of a wind farm could be doubled by installing an FPV system which takes up only 20% of the total farm area.

The levelised cost of energy (LCOE) of offshore wind is one of the obstacles to its wider adoption [22,23]. The co-location of offshore wind and solar can decrease the levelised cost of energy (LCOE) through the shared use of infrastructure, such as moorings and substructures, submarine cables and substations, as well as operational resources like crews and vessels for maintenance (O&M) activities, which represent a significant portion of costs of an offshore project [24]. Additionally, this co-location can support aquaculture production and potentially contribute to ecosystem restoration, further enhancing the environmental compatibility of offshore energy projects [25].

Existing research on hybrid wind-solar energy systems has primarily concentrated on examining the complementarity between wind and solar resources resources and the resulting potential for power smoothing. For instance, Canul-Reyes et al. [26] examined this for the Yucatan peninsula in Mexico, Li et al. [27] in seas of China, Hou et al. [28] in Ordos, China and Schindler et al. [29] in Germany, among many other studies [30–34]. Other works have examined how the solar to wind installation capacity effects the complementary and variability of the in-situ energy generation [10,35]. However, there is a gap in the research regarding the impact of the tilt angle of the FPV system on the energy output variability of a hybrid site, particularly in determining the optimal tilt angle for minimising variability. There are numerous studies exploring the optimal tilt angle for maximising solar irradiance incident on PV modules, thereby enhancing solar energy generation, with extensive literature covering a wide range of locations such as Turkey Turkey [36–38], Egypt [39] and Bangladesh [40].

Kapica et al. [41], investigated the complementarity between offshore wind and solar PV under three tilt angle scenarios across global onshore regions using daily-resolution data. Their findings indicate that the impact of solar tilt angle on wind–solar complementarity is location-dependent, with negligible effects in some regions and more pronounced influences in others. However, there remains a research gap regarding the impact of the tilt angle of FPV systems on the energy output variability of a hybrid site. This research question, which may also be formulated as the optimisation of tilt angle to minimise variability in hybrid systems, is the focus of the present work.

This work offers a novel approach by assessing the variability of the FPV system deployed at 121 distinct tilt angles, ranging from 0 to 60 degrees in 0.5-degree increments. Within the solar energy field, a commonly applied guideline suggests that the optimal fixed tilt angle for a photovoltaic panel is typically 10°–15° above the local latitude in winter and 10°–15° below the latitude in summer [42,43]. Yunus Khan et al. [44] conducted a comprehensive synthesis of prior research, categorising studies into mathematical modelling, experimental, and simulation-based approaches. Their findings indicate that regions near the equator (0° latitude) typically exhibit optimal tilt angles up to 2.5°. For latitudes between 2.6° and 30°, optimal tilt angles range from 5° to 28°, while regions between 40° and 70° latitude demonstrate optimal tilts of approximately 29° to 40°.

Previous investigations into optimal tilt angles have generally considered the full range from 0° to 90°. Examples include Božiková et al. for a PV system in Brno, Czechia; Abed and Al-Salami [30] for all provinces of Turkey; Memon et al.for a 1 MW solar PV installation in Pakistan; and Ali Morad et al. [45] for multiple cities in Iraq. In contrast, the present study limits the tilt range to 0°–60°, with a high resolution of 0.5°, in order to account for the increased wind loads associated with larger tilt angles in FPV systems [46,47].

Chou et al. [48] demonstrated that critical wind loads on FPV panels are more likely at lower wind incidence angles and at tilt angles exceeding 30°, based on an assessment covering tilt angles from 10° to 80° and wind incidence angles from 0° to 180°. Accordingly, a maximum tilt of 60° is adopted in this study. Importantly, the objective is not to maximise solar energy yield in isolation, but to identify the tilt angle that optimises complementarity between wind and solar generation. Specifically, this study determines the optimal tilt angle for an FPV system retrofitted to two existing offshore wind farms, with the aim of minimising variability in hybrid energy production across hourly, daily, and monthly timescales.

The paper is structured as follows. Section 2 introduces the two offshore wind farms selected for the study. It includes an overview of the data obtained from the ERA5 reanalysis dataset, which is used to calculate both solar and wind energy. A specific PV module model is chosen for the solar energy calculation, while the power curves of the wind farm's turbines are used to estimate the wind energy. This section also presents the method for calculating the tilted surface irradiance from horizontal irradiance. Next, the metric used to quantify the variation in the energy output is discussed. In section 3, the results for the analysis on three different time resolutions are presented and discussed. Finally, conclusions are drawn in Section 4.

2. Study sites

The analysis was conducted on two existing offshore wind farms, Westermost Rough (WMR) (U.K.) and South Fork (SFK) (U.S.), selected for their potential to be retrofitted with floating solar photovoltaic (FPV) arrays. While previous research, notably [10], has examined the impact of FPV capacities relative to wind farm capacity on energy output variability, this study is the first to investigate how the tilt angle of deployed FPV systems influences energy output variability. The latitude difference of over 12 degrees between these sites provides an opportunity to investigate whether the tilt angle, determined by latitude, influences the variability of the total wind and solar energy production at different geographical locations.

The WMR wind farm is situated approximately 8 km off the east coast of Yorkshire, north of Hull [49]. The project was the first offshore wind farm in the world to commercially deploy the large-scale Siemens SWT-6–154 6 MW wind turbines, with a total of 35 units [50,51]. The construction of the 210 MW project commenced in April 2013, with the final turbine installation completed in March 2015 [52]. The project was fully commissioned in May of the same year [53]. At the time of commissioning, WMR represented approximately 4% of the total installed offshore capacity in the UK; however, this figure had decreased to around 1% by 2023 [54].

Commissioned in May 2024, SFK is the second commercial-scale offshore wind farm in the U.S. Its inauguration marks a significant

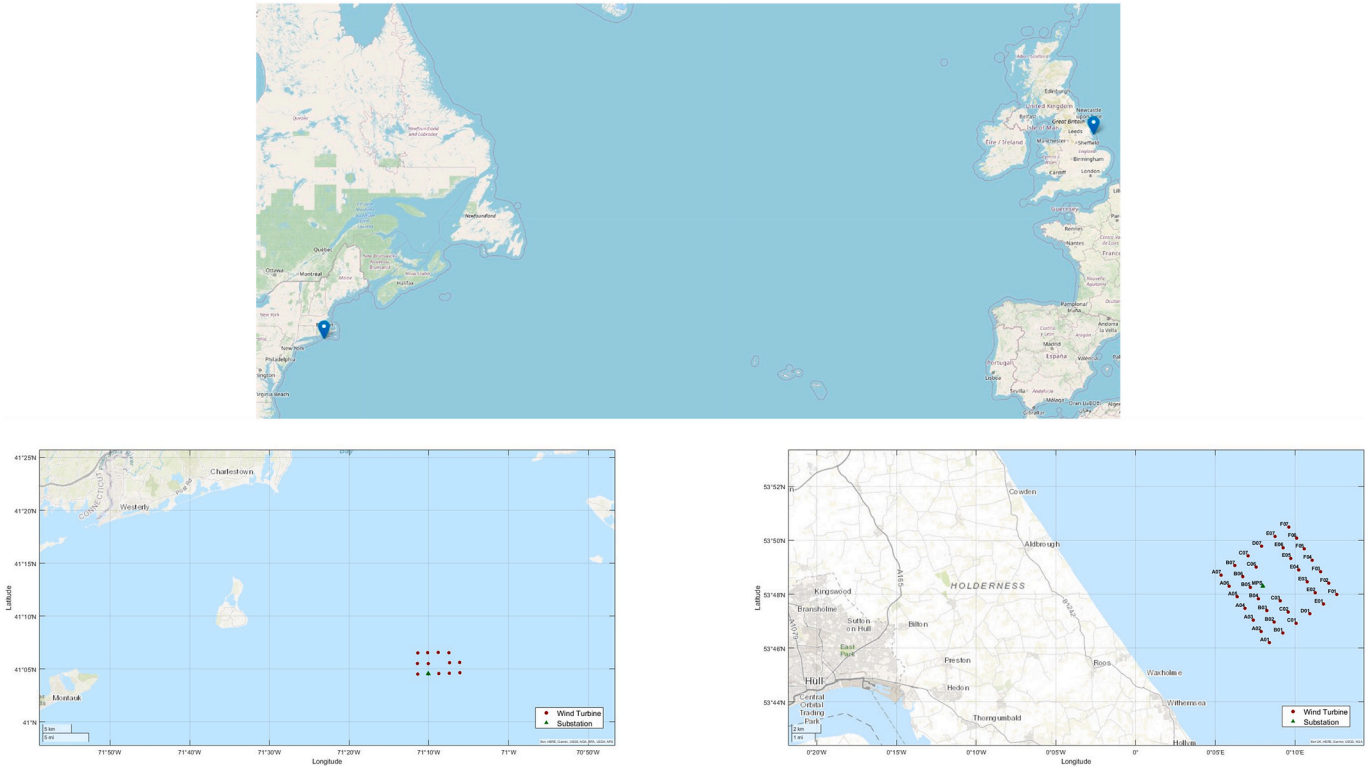


Fig. 1. South Fork (left) and Westermost Rough (right).

Table 1
Studied offshore wind farms [59–63].

	Symbol	Units	Westermost Rough	South Fork
Country			United Kingdom	United States
Coordinates			53°48′09″N, 0°08′31″E	41°5.517′N, 71°10.073′W
Capacity	P_r	MW	210	132
Number of wind turbines			35	12
Hub height		m	102	144
Wind turbine model			Siemens SWT-6.0–154	Siemens Gamesa SG11.0–200 DD
Annual energy output		GWh	890	540
Capacity factor	CF		0.483	0.47
Export capacity	C_G	MVA	212	150
Area	A_w	km^2	35	30
Water depth	D_w	m	16–26	33–41
Distance to shore	D_s	km	8	30

Table 2
Wind turbine specifications [64–67].

	Symbols	Units	SiemensSWT-6.0–154	Siemens Gamesa SG11.0–200 DD
Rotor diameter		m	154	200
Swept area		m^2	18,600	31,400
Nominal power	P_n	MW	6	11
Cut-in wind speed	u_i	m/s	4	4
Cut-out wind speed	u_o	m/s	25	32
Rated wind speed	u_n	m/s	13	14
Power regulation			Pitch	Pitch

milestone for the U.S. offshore wind industry, which has faced challenges such as supply chain disruptions and limitations in port and vessel infrastructure [55]. The 132 MW wind farm, located 56 km east of Montauk Point, New York, produces enough clean energy to power around 70,000 Long Island homes annually [56,57]. The site features 12 Siemens Gamesa 11 MW turbines, aligning with the industry trend of utilising fewer, higher-capacity turbines to reduce the project's levelised cost of energy (LCOE) [58] Fig. 1.

3. Materials and methods

3.1. Wind farm data

Table 1 outlines the key characteristics of both sites, while Table 2 summarises the technical specifications of the two installed wind turbine models. Fig. 2 illustrates the power curves for both turbines. Due to the limited data available on the Gamesa SG 11.0–200 DD wind turbine, this study used a scaled model based on the power curve of the similar Vestas V164/9500 9.5 MW turbine. The curve's shape was preserved while being proportionally adjusted by a scaling factor of 11/9.5 to reflect the higher capacity of the Gamesa turbine.

3.2. Climate data

The required climatic parameters for this study were obtained from the Copernicus ERA 5 reanalysis dataset, the fifth generation European for Medium-Range Weather Forecasts (EXMWF), covering the period from 1940 to the present. Reanalysis integrates past weather observations with an atmospheric model to reconstruct previous global weather conditions. ERA 5 reanalysis provides hourly gridded data with a spatial resolution of 31 by 31 km. The ERA5 dataset is publicly available through the Copernicus Climate Data Store (CDS) [68] which offers a user-friendly interface for accessing and downloading the data. As a

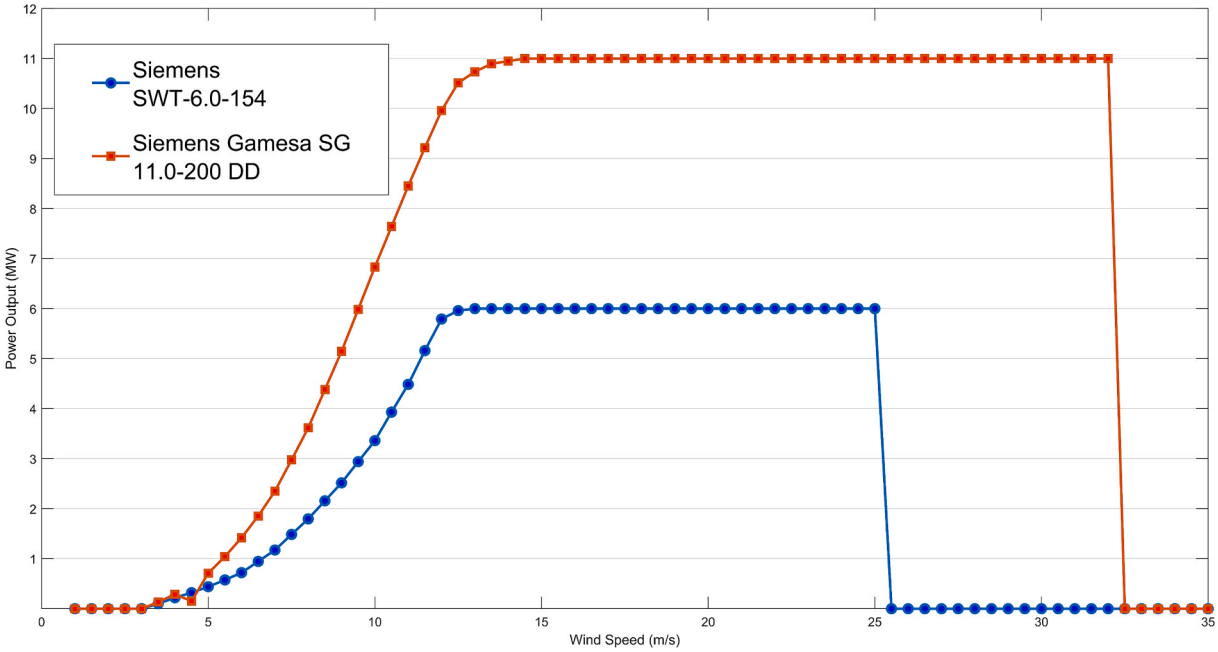


Fig. 2. Wind turbine power curves.

Table 3
Parameters from the ERA5 dataset used in this study [73].

Dataset Variable	Symbol	Unit
Global solar irradiance incident on a horizontal surface	G	W/ m^2
Direct solar irradiance incident on a horizontal surface	G_b	W/ m^2
Ambient air temperature 2 m above the sea surface	T_a	°C
Sea surface temperature	T_w	°C
Surface albedo	ρ	–
Eastward and northward components of wind velocity at a height of 10 *m*	v_{x10}, v_{y10}	m/s
Eastward and northward components of wind velocity at a height of 10 *m*	v_{x100}, v_{y100}	m/s

Table 4
PV module specifications [77].

	Unit	Symbol	Quantity
Peak Power at STC	W	P_R	405.0
Weight	kg	m	21.0
Dimensions	mm		1754 x 1096
Temperature Coefficient	$°C^{-1}$	γ	−0.34%

Table 5
Site installation capacities.

	Symbol	Unit	WMR	SFK
Solar capacity	C_S	MW	273	171.6
Hybrid site capacity	C_H	MW	483	303.6
No. modules	*n*		674,075	423,704

Table 6
Farm capacity factors over study period.

	Symbol	WMR	SFK
Wind capacity factor	CF_W	44.33%	48.61%
Solar capacity factor, β = 0°	CF_S	11.98%	16.73%
Hybrid capacity factor	CF_H	26.05%	30.59%

result, ERA5 has become a popular choice for researchers around the world, especially in fields related to renewable energy and climate modelling. In recent years, the ERA5 dataset has been applied in advanced research on optimising solar PV tilt angles [69] and examining the complementary relationship between solar and wind energy resources [70]. In this study, we opted for the ERA 5 reanalysis over other available reanalysis resources, such as MERRA 2 by NASA, because ERA 5 outperforms MERRA 2 in wind energy modelling [71] and solar irradiance estimation [72]. Table 3 displays all the parameters obtained from ERA5 for this research.

The dataset spans 11 years, from January 1, 2014, to December 31, 2024, with an hourly time resolution. Although WMR was commissioned in 2015 and SFK in 2024, we carried out the investigation as if both wind farms were commissioned at the beginning of 2014. This assumption allowed us to analyse the impact of variability in energy output from both sites when combined with a Floating Photovoltaic (FPV) installation of a specific capacity. We compared the hybrid solar-wind energy output to wind-only output and examined how the FPV system's tilt angle affects variability at the hybrid site.

3.3. Photovoltaic technology

Recent years have seen increased interest in Perovskite solar cells due to advancements in efficiency and their tuneable bandgap. However, silicon-wafer-based PV technology still dominates the global market, accounting for around 97% of the total production worldwide, making crystalline silicon cells the technology of choice for this study [74].

There are three types of crystalline silicon solar cells: monocrystalline, polycrystalline, and amorphous silicon, with monocrystalline and polycrystalline being the most commonly used. Monocrystalline solar cells have a single continuous crystalline lattice structure, and they are manufactured using a process known as the Czochralski process [75]. Polycrystalline cells contain multiple silicon layers that are melted together during their less complex manufacturing process. Monocrystalline cells have a higher efficiency than their polycrystalline counterpart, with an efficiency between 20 and 25%, which is superior to the efficiency of polycrystalline cells, which have an efficiency between 13 and 16% [76].

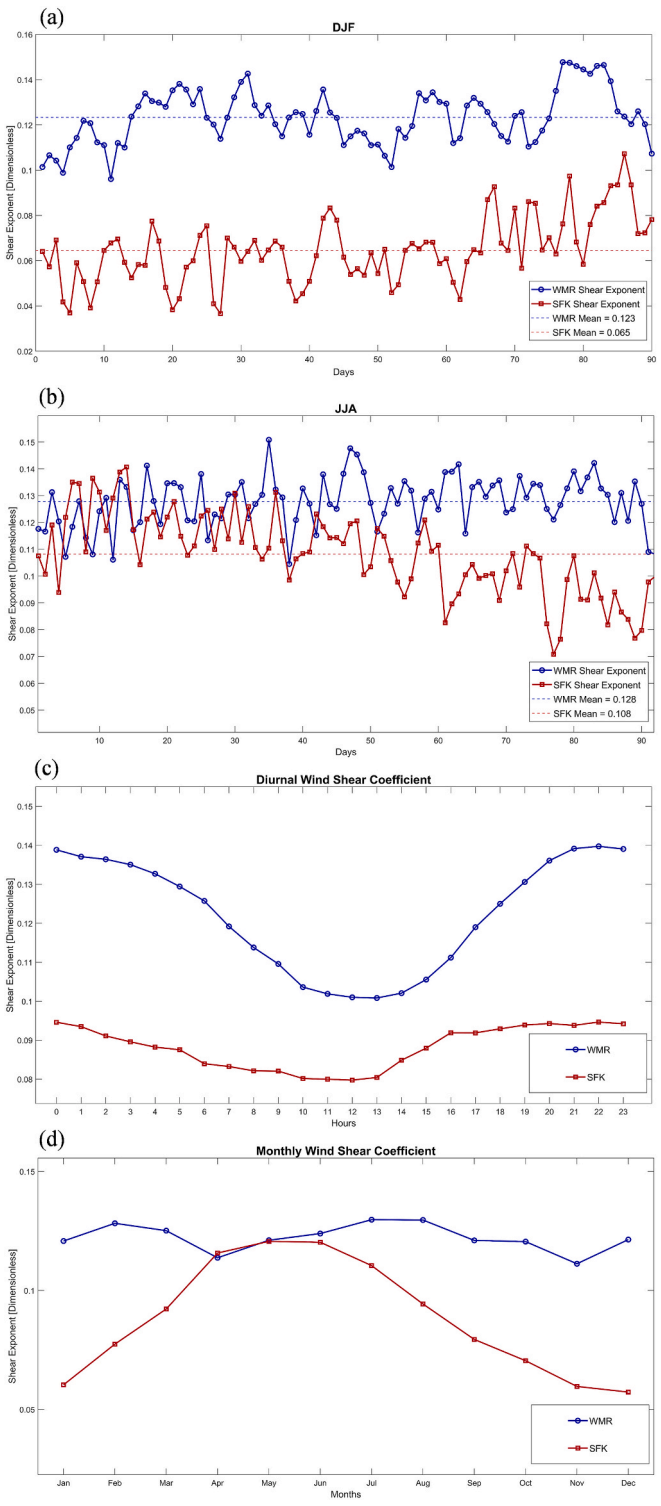


Fig. 3. Average wind shear coefficient at both sites: (a) daily average for December-January-February, (b) daily average for June-July-August, (c) average diurnal cycle, (d) average seasonal variation.

The Trina TSM-405DE09 405 W monocrystalline photovoltaic module was selected for this study based on its high efficiency. It is assumed to be installed on a pontoon-type floating platform, with mooring lines anchored to fixed points. Table 4 displays the key performance parameters of the module under Standard Test Conditions.

A study by [10] examined the ideal solar-to-wind installation capacity for reducing energy output variability in three offshore wind farms that integrated FPV systems. The findings revealed that the optimal ratio varied significantly across hourly, daily, and monthly timescales. To ensure that all timescales were considered equally, a parameter was derived to assess the optimal solar-to-wind capacity ratios, which were determined to be 1.4:1, 1.24:1, and 1.1:1, respectively. Therefore, the solar-to-wind installation capacity was maintained at a ratio of 1.3:1 for both wind farms throughout this study. Table 5 presents the chosen capacities of the FPV systems to be installed at WMR and SFK.

3.4. Solar energy

The solar irradiance incident on a horizontal surface, G is the sum of the horizontal beam irradiance, G_b and the horizontal diffuse irradiance G_d:

$$G = G_b + G_d. \tag{1}$$

Various models of different complexity are used to translate horizontal irradiances onto tilted planes. The HDKR (Hay–Davies–Klucher–Reindl) anisotropic model was employed in this study due to its established reliability and common application in commercial solar calculators. The model assumes that there are three components of diffuse irradiance: an isotropic component, evenly distributed across the sky; a circumsolar component, concentrated in the region of the sky near the sun; and a horizon brightening component, originating from the area of the sky near the horizon [78,79]. The following equation represents the HDKR model:

$$G_T = G_{T,b} + G_{T,d} + G_{T,ref} \tag{2}$$

where G_T is the global irradiance on a tilted surface, $G_{T,b}$ is the tilted beam irradiance, $G_{T,d}$ is the tilted diffuse irradiance and $G_{T,\,ref}$ is the is the irradiance reflected from the ground onto the tilted surface [79,80].

The beam irradiance on a tilted surface is calculated as:

$$G_{T,b} = G_b R_b\,, \tag{3}$$

where R_b is the beam irradiance ratio defined as the ratio of beam irradiance incident on a tilted surface to that on a horizontal surface [81]. For the northern hemisphere R_b can be calculated as:

$$R_b = \frac{\cos(\theta)}{\cos(\theta_z)}, \tag{4}$$

where θ_z is the zenith angle and θ is the angle of incidence on the tilted surface, both of which can be calculated as:

$$\cos(\theta) = \cos(\phi-\beta)\cos(\delta)\cos(\omega) + \sin(\phi-\beta)\sin(\delta), \tag{5}$$

$$\cos(\theta_z) = \cos(\phi)\cos(\delta)\cos(\omega) + \sin(\phi)\sin(\delta). \tag{6}$$

In these equations, ϕ denotes the location's latitude, β is the angle of tilt of the PV module, ω is the hour angle and δ is the solar declination angle [81–83].

The diffuse irradiance on a tilted surface is determined using the following equation:

$$G_{T,d} = G_d\left[(1-A_i)\left(\frac{1+\cos(\beta)}{2}\right)\left(1+fsin^3\left(\frac{\beta}{2}\right)\right)+A_iR_b\right], \tag{7}$$

where A_i, the anisotropy index, is defined as the ratio of beam irradiance on a horizontal surface to extraterrestrial irradiance, G_o, with higher values indicating the greater circumsolar contribution [78]. The anisotropy index is expressed as:

$$A_i = \frac{G_b}{G_o}. \tag{8}$$

In Eq. (7), f is the horizon brightening factor [80], given by:

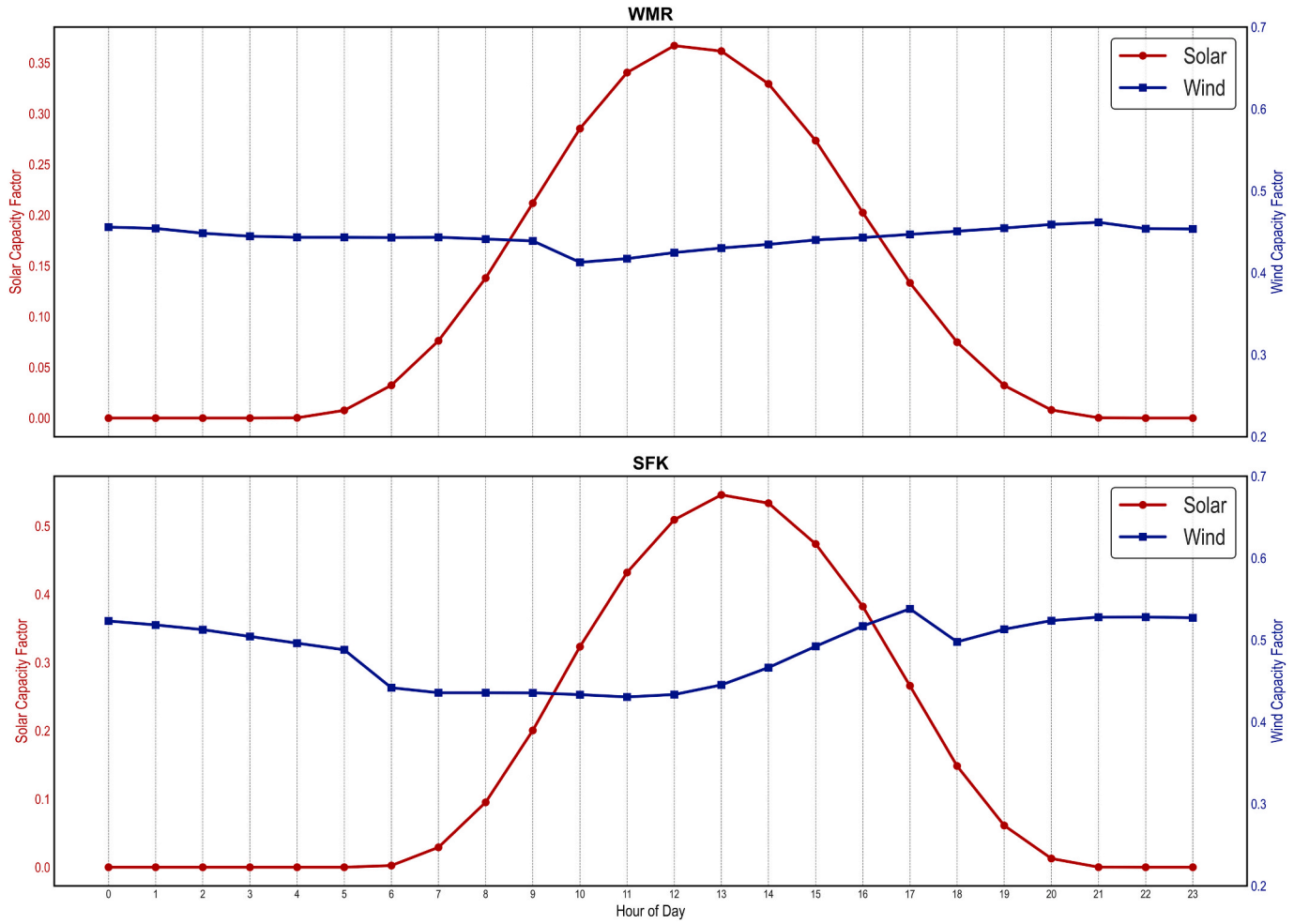


Fig. 4. Average daily capacity factors for solar (left axis, with β = 0°) and wind (right axis) over the 11-year study period, shown for WMR (top) and SFK (UTC–4, bottom).

$$f = \sqrt{\frac{G_b}{G}}. \tag{9}$$

The ground-reflected irradiance is calculated by:

$$G_{T,ref} = G\rho\left(\frac{1-\cos(\beta)}{2}\right), \tag{10}$$

where $G_{T,ref}$ is the ground-reflected irradiance on the tilted surface (Wm^{-2}), G is the global horizontal irradiance (Wm^{-2}), ρ represents the sea surface albedo (dimensionless) and β is the tilt angle of the photovoltaic module (°). Rather than assuming a constant value, the ERA5 surface albedo parameter was used directly as an hourly input variable (Table 3). Typical ocean albedo values range from 0.06 to 0.4 [84].

The power output of the photovoltaic module was calculated using the model from [85], which accounts for the influence of module temperature and solar irradiance on performance as follows:

$$P_s = P_{STC}\frac{G_T}{G_{STC}}[1-\gamma(T_M - T_{STC})], \tag{11}$$

Where P_s is the module output power (W), P_{STC} is the module maximum rated power at standard test conditions (STC) (W), G_T is the calculated total irradiance on the tilted surface (Wm^{-2}), G_{STC} is the solar irradiance intensity at STC (Wm^{-2}), T_{STC} is the module temperature at STC (°C), T_M is the module operating temperature (°C), and γ is the solar module temperature coefficient of power ($°C^{-1}$) [10,85]. Since both sites are located in the Northern Hemisphere, the FPV systems were assumed to face towards the equator (south-facing) throughout the study, corresponding to an azimuth angle of 0°.

Numerous research papers consistently indicate that FPV systems are more efficient and generate more electricity than land-based systems, primarily due to the cooling effect of water [86]. Given that the FPV systems in this study will be deployed over the ocean, the model derived by [87] was implemented to estimate the FPV module operating temperature, T_M. This model incorporates the effects of irradiance, ambient air temperature, wind speed, and seawater temperature, as described below:

$$T_M = e_0 + e_1 T_a + e_2 G_T - e_3 v_w + e_4 T_w, \tag{12}$$

where T_a is the ambient air temperature, G_T is the solar intensity on the tilted surface, v_w is the wind velocity and T_w is the water temperature [87]. The least-squares minimisation theorem was used to elicit the parameters: $e_0 = 1.8081$ ∘C, $e_1 = 0.9282$, $e_2 = 0.021$ ∘C m^2 W^{-1}, $e_3 = 1.2210$ ∘C m^{-1} s and $e_4 = 0.0246$ [10,87].

The solar energy output of a single module, $E_{\bar{S}}$, is calculated by integrating the output power P_s, over a one-hour interval shown in Equation (13). Thus, the total daily energy output is the sum of 24 consecutive hourly energy values, and so on. The total solar energy output from the entire site is simply the energy from one module, scaled by the number of modules on site, denoted by E_S:

$$E_{\bar{S}} = \sum_n P_S \Delta t. \tag{13}$$

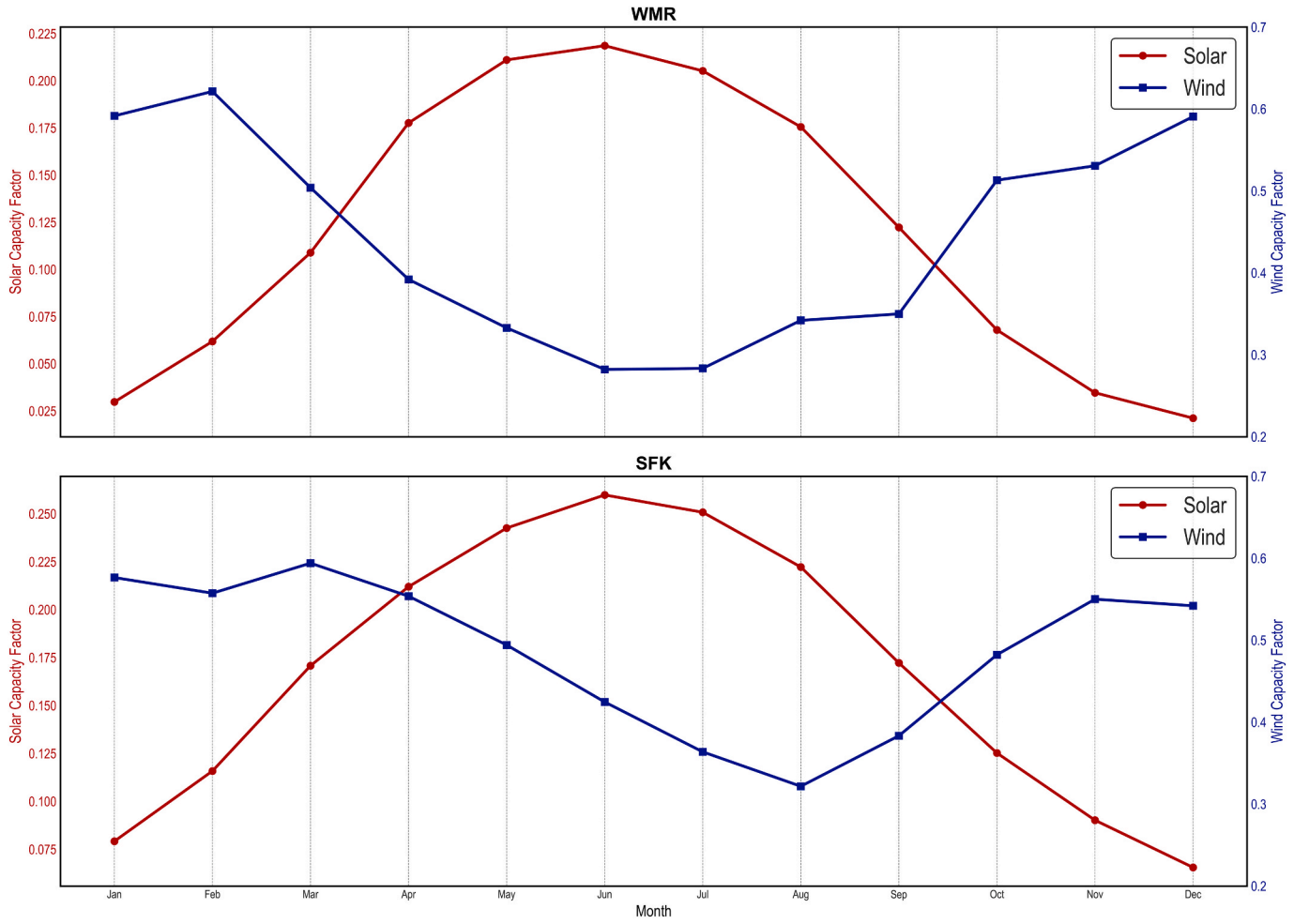


Fig. 5. Average monthly capacity factors for solar (left axis, with $\beta = 0°$) and wind (right axis) over the 11-year study period, shown for WMR (top) and SFK (bottom).

3.5. Wind energy

Wind velocity data were obtained from the ERA5 reanalysis dataset, which provides wind velocity measurements at two heights: 10 m and 100 m above the earth's surface. The wind speeds at both heights, v_{10} and v_{100}, are obtained from their eastward and northward velocity components:

$$v_{10} = \sqrt{v_{x10}^2 + v_{y10}^2}, \tag{14}$$

$$v_{100} = \sqrt{v_{x100}^2 + v_{y100}^2}. \tag{15}$$

To determine the wind speeds at the hub heights of the two study sites, a vertical extrapolation technique was applied. Various methods exist in the literature for extrapolating wind speed to the hub height of a wind turbine. The Wind Power Law, being the most commonly used method, was employed in this study.

The Power Law is given by

$$\frac{v_2}{v_1} = \left(\frac{h_2}{h_1}\right)^{\alpha}, \tag{16}$$

where v_2 and v_1 represent the wind velocity at heights h_2 and h_1 respectively, and α is the wind shear coefficient. Higher values of α signify a greater change in wind speeds with altitude. A value of 0.14 is typically assumed for α. However, α is not a constant; it varies based on several factors, including temperature, pressure, humidity, time of the day, season, wind velocity and terrain type [88]. The simplistic assumption of the constancy of α can lead to discrepancies in electricity generation of up to 50% when comparing actual electricity generation with estimated generation derived from vertical extrapolation using a constant α [88]. To reduce the potential errors that may arise from using a constant α, we calculated α based on the hourly wind velocity measurements at heights of 10 m and 100 m:

$$\alpha = \frac{\ln\left(\frac{v_{100}}{v_{10}}\right)}{\ln(10)}. \tag{17}$$

The wind shear coefficient thus calculated was used to estimate the wind velocity at the hub heights of 102 m and 144 m.

The power output of both turbine models can be determined by matching the wind speed at hub height to the power curves shown in Fig. 2. To evaluate the instantaneous power output of a turbine at wind speeds that fall between the points on its power curve, linear interpolation was employed. The wind energy output from a single turbine, $E_{\overline{w}}$, is calculated by integrating the power output over a one-hour interval. Thus, the total daily energy output is the sum of 24 consecutive hourly energy values, and so on:

$$E_{\overline{w}} = \sum_{n} P_w \Delta t. \tag{18}$$

The total wind energy output from the entire wind farm is simply the

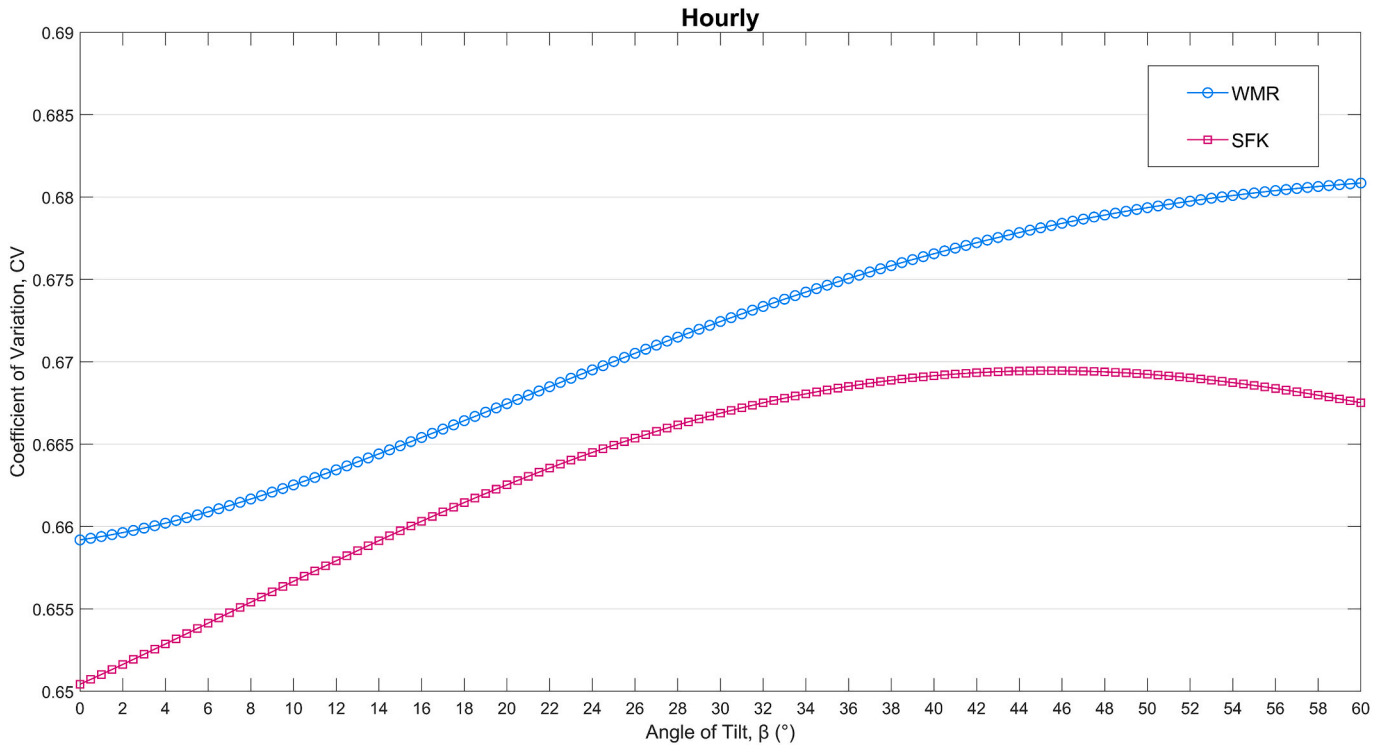


Fig. 6. Coefficient of variation of the hybrid farms for different tilt angles across the 11-year study period, calculated on an hourly timescale.

energy from one turbine, scaled by the number of turbines on site; it is denoted in this work by E_w. The capacity factor of wind energy, $CF_{W,}$ is the ratio of the actual energy produced to the energy that would have been produced if all turbines had operated at their rated power over a specified period.

The total energy output from the hybrid farm, denoted as E_H, is the sum of the wind energy output (E_w) and the solar energy output (E_S). Similarly, the capacity factor of the hybrid farm, CF_H, is the ratio of the actual hybrid energy output over a given period of time to the hypothetical energy that would have been produced if the hybrid farm had operated at full capacity during the period considered. Table 6 provides the capacity factor for both wind farms, the capacity factor for the FPV systems alone, and the capacity factor for the hybrid farms throughout the 11-year study period.

The global average offshore wind capacity factor, 41% [89], is amply exceeded by both wind farms, WMR and SFK (Table 6), which attests to the substantial potential of the sites for wind energy generation. The solar capacity factors are lower, which reflects a somewhat weaker potential for solar energy generation, which is to be expected given the latitude. Notwithstanding, the retrofitting of the wind farm with solar PV energy to create hybrid farms has significant benefits, on which more, below. The capacity factors of the hybrid farms are in between those of the wind and solar subsystems.

3.6. Coefficient of variation

The coefficient of variation (CV) of the energy output was calculated for both sites with the FPV installation at different tilt angles. The CV is a statistical measure of the dispersion of data points in a data series around the mean and can be calculated using

$$CV = \frac{\sigma}{\mu}, \tag{19}$$

where σ is the standard deviation and μ is the mean of the time series. This metric has been used in the literature to quantify output variability in offshore hybrid systems combining wind with wave [90] or solar energy [10,91,92].

In this study, we will calculate the CV for the energy output of the hybrid farm, denoted as E_H. A lower CV indicates less fluctuation, which may be expected to lead to fewer balancing actions by grid operators, which in turn can lower balancing costs. These savings may ultimately be reflected in reduced electricity prices for consumers [93]. As mentioned above, the objective is to determine the angle of tilt that results in the lowest variability, or in other words, in the "smoothest" energy output. This analysis will be conducted across three-time scales: hourly, daily, and monthly, with the rationale explained below.

3.7. Correlation metrics

The relationship between solar and wind energy generation is quantified using the Pearson correlation coefficient r, defined as

$$r_{X,Y} = \frac{\mathrm{cov}(X, Y)}{\sigma_X \sigma_Y} \tag{20}$$

where $\mathrm{cov}(X, Y)$ is the covariance between the variables X and Y, and σ_X and σ_Y are their standard deviations. The coefficient is a parametric measure used to quantify the strength and direction of the linear relationship between two continuous variables. The value of r ranges between -1 and 1, where 1 indicates a perfect positive linear relationship, -1 indicates a perfect negative linear relationship, and 0 indicates no linear correlation. The magnitude of the coefficient reflects the strength of the association, while the sign indicates whether the relationship is positive or negative [94,95]. Positive values of r indicate synchronous variation between the two resources, while negative values suggest complementary behavior, meaning that when one resource peaks the other tends to decline, which can be advantageous in hybrid solar and wind systems as it helps reduce overall variability in power generation [11,92].

Kendall's tau τ is a non–parametric rank correlation coefficient that measures the strength and direction of a monotonic association between two variables. It is defined as:

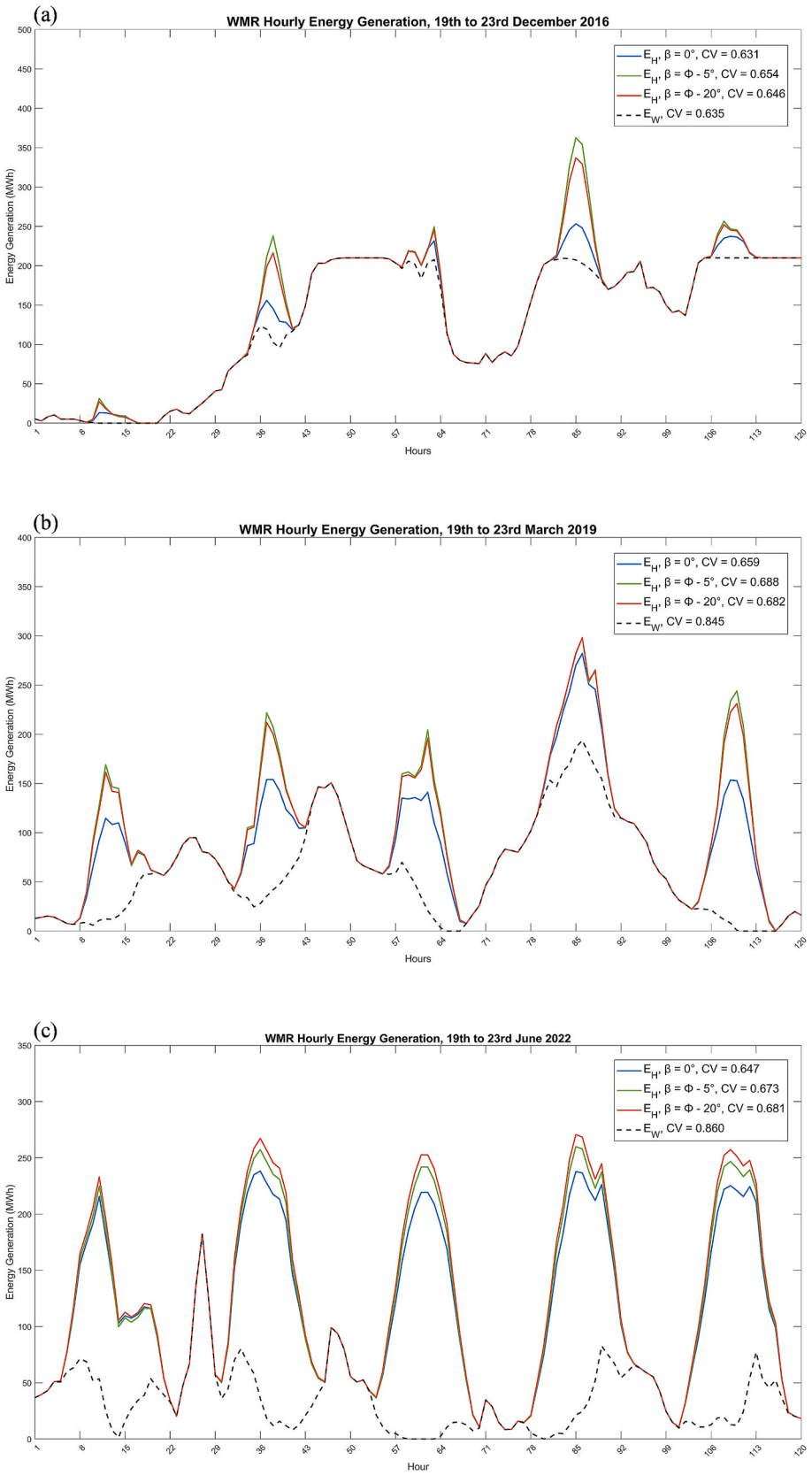


Fig. 7. Coefficient of variation of the hybrid site energy generation and wind-only energy generation for three tilt angles at WMR: (a) hourly, winter solstice 2016; (b) hourly, march equinox 2019; (c) hourly, summer solstice 2022.

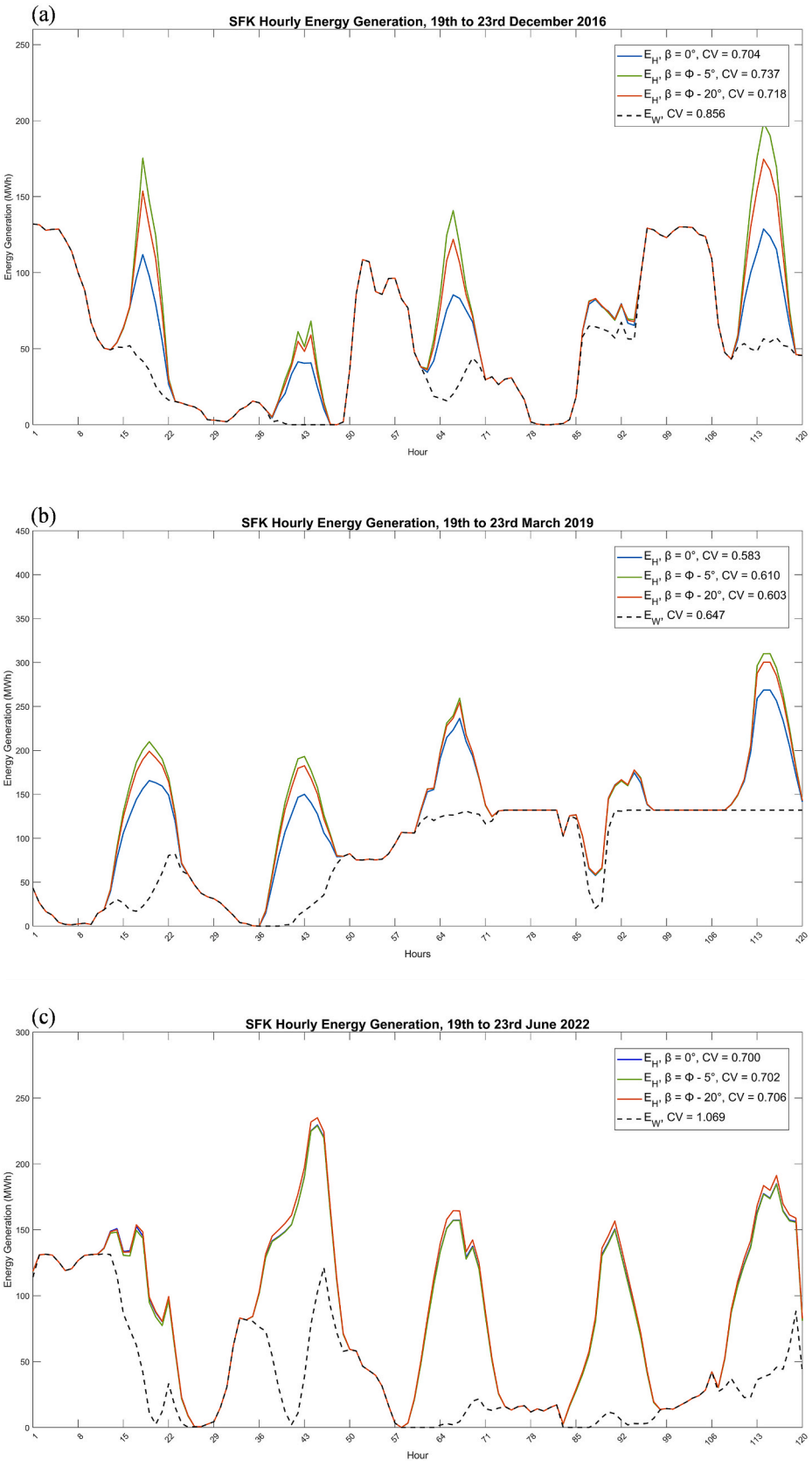


Fig. 8. Coefficient of variation of the hybrid site energy generation and wind-only energy generation for three tilt angles at SFK: (a) hourly, winter solstice 2016; (b) hourly, March equinox 2019; (c) hourly, summer solstice 2022.

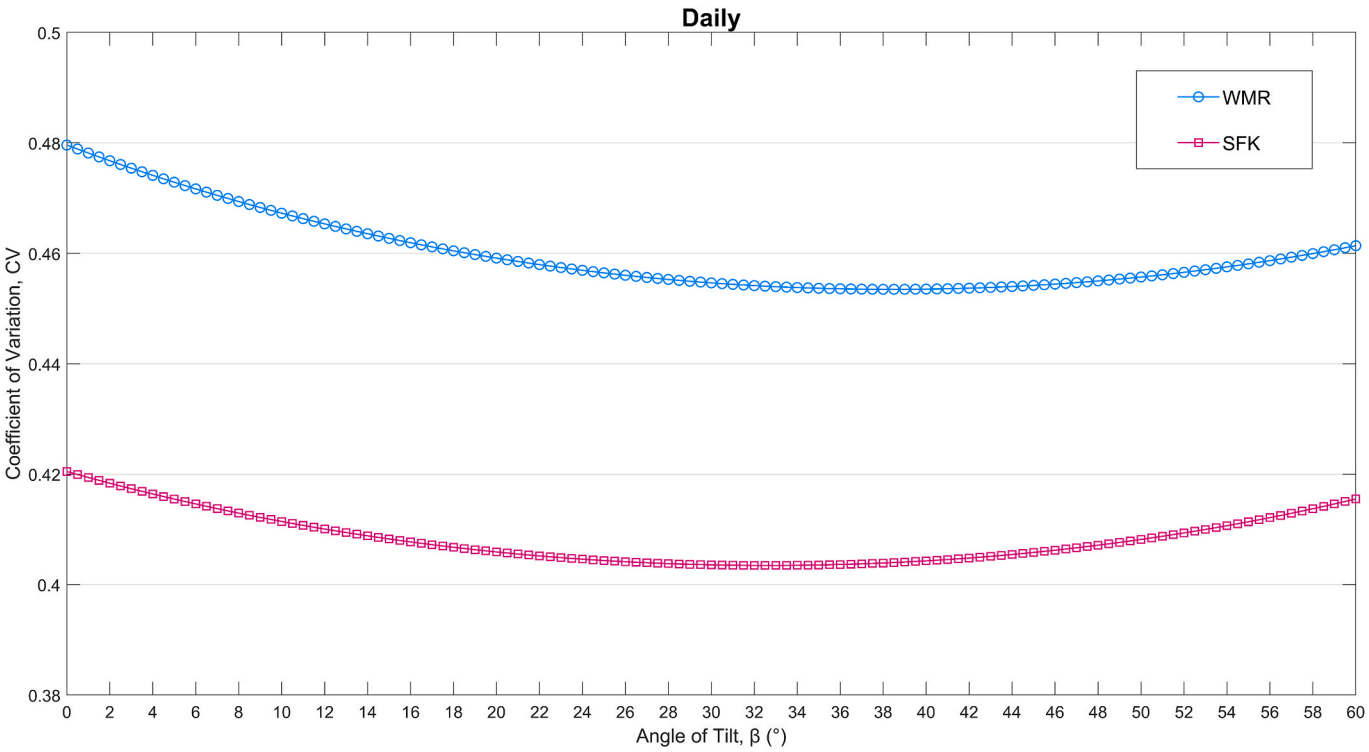


Fig. 9. Hybrid energy coefficient of variation of the hybrid farms for different tilt angles across the 11-year study period, calculated on a daily timescale.

Table 7
The angle of tilt for the maximum hybrid capacity factor, $\beta\{CF_{H,max}\}$, and for the minimum coefficient of variation based on hourly, $\beta\{CV_{min}^{(h)}\}$, daily, $\beta\{CV_{min}^{(d)}\}$, or monthly, $\beta\{CV_{min}^{(m)}\}$, timescales.

		SFK	WMR
	ϕ	41.1°	53.8°
	$\beta\{CF_{H,max}\}$	35.5°	43.5°
Hourly	$\beta\{CV_{min}^{(h)}\}$	0.0°	0.0°
Daily	$\beta\{CV_{min}^{(d)}\}$	32.5°	38.5°
Monthly	$\beta\{CV_{min}^{(m)}\}$	40.5°	28.0°

Table 8
Minimum coefficient of variation for the hybrid farms (CV_{min}) compared to wind-only farms (CV_W) at different temporal resolutions, denoted by the superindices h (hourly), d (daily) and m (monthly).

		SFK	WMR
	ϕ	41.1°	53.8°
	$CF_{H,max}$ [β]	32.33% [35.5°]	27.98% [43.5°]
Hourly	$CV_{min}^{(h)}$ [β]	0.65 [0.0°]	0.66 [0.0°]
	CV_W	0.77	0.82
Daily	$CV_{min}^{(d)}$ [β]	0.40 [32.5°]	0.45 [38.5°]
	CV_W	0.61	0.7
Monthly	$CV_{min}^{(m)}$[β]	0.12 [40.5°]	0.14 [28.0°]
	CV_W	0.21	0.32

$$\tau = \frac{C - D}{C + D} \tag{21}$$

where C denotes the number of concordant pairs and D denotes the number of discordant pairs. A pair of observations is considered concordant when the relative ordering of the two observations is the same for both variables, and discordant when the order differs between variables. Similar to the Pearson coefficient, the value of Kendall's τ ranges between -1 and 1, where 1 indicates perfect agreement, -1 indicates perfect disagreement, and 0 indicates no association between the ranked variables.

Kendall's τ is particularly well suited to the analysis of wind and solar energy data, where relationships are often monotonic but not strictly linear. Consequently, it has been widely applied in renewable energy studies. For example, it has been used to examine wind–solar resource complementarity under climate change scenarios in China [96], as well as offshore wind–solar resource complementarity [27]. Additionally, [97] employed Kendall correlation as part of its analysis of environmental drivers affecting photovoltaic performance.

4. Results & Discussion

4.1. Wind shear coefficients

This section will briefly overview the calculated α values observed during the study period. The daily average α values for the average year significantly vary from the common estimate of 0.14, both spatially and temporally. During the winter months, SFK had a lower α value than WMR, averaging 0.065 compared to WMR's 0.123, as depicted in Fig. 3. However, in the summer months, SFK's α values increased significantly, while WMR's remained consistent, resulting in average values of 0.108 for SFK and 0.128 for WMR. Approximately 62% of the hourly α values at WMR fall below 0.14. At SFK, 77% of the hourly α values were below 0.14. This aligns with the findings of [98], which indicated that over 80% of α values offshore were below 0.14, primarily due to the smoother surface of the water compared to land. Both sites have a consistent diurnal pattern to previous studies with the highest α values being experienced during the night time because of the development of stable atmospheric conditions during the night, leading up to sunrise, due to surface cooling [98]. However, the seasonal variation differs from typical findings in on-land research, where the highest α values are generally recorded during the winter months. In contrast, for the two study sites, the highest α values are observed in the summer.

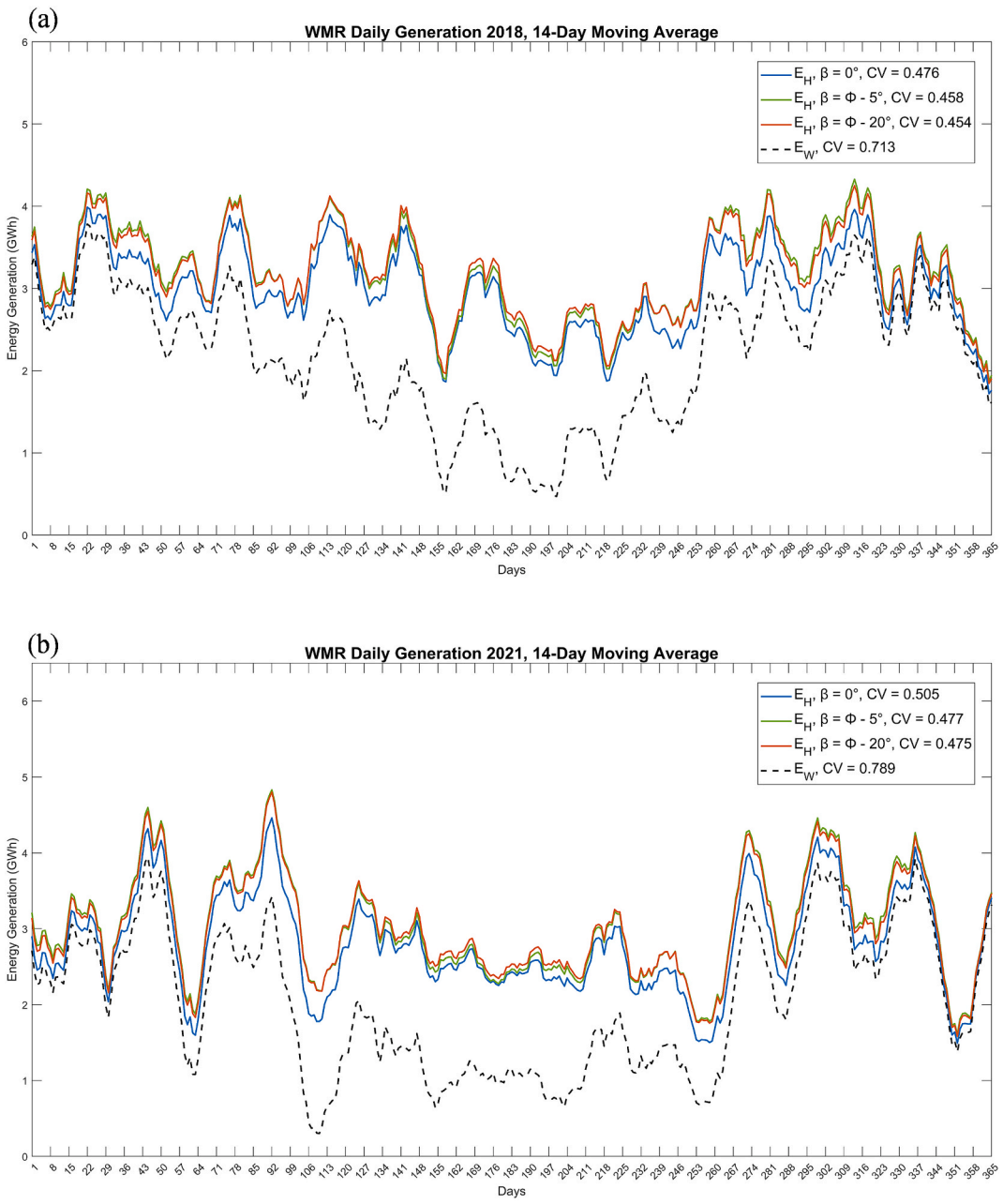


Fig. 10. Coefficient of variation of the hybrid site energy generation and wind-only energy generation for three tilt angles at WMR: (a) daily, 2018; (b) daily, 2021.

4.2. Seasonal and diurnal generation

Complementary generation patterns are evident on both diurnal (Fig. 4) and seasonal (Fig. 5) timescales. At both sites, solar generation peaks around midday, while wind generation tends to be stronger during the night and early morning, with slight reductions throughout the day. As this represents the 11-year daily average, short-term (hour-to-hour) variability is largely smoothed out.

On the seasonal scale, the complementary relationship becomes more pronounced. For example, at WMR in June, the average monthly wind capacity factor reaches its second-lowest value of 28.2%, coinciding with the highest solar capacity factor of 21.9%. Conversely, in the winter months, solar output declines sharply (with a minimum capacity factor of 2.1% in December), while wind output peaks (reaching 62.1% in February). A similar trend is observed at SFK, where maximum solar generation occurs in June and the lowest wind generation is recorded in August.

4.3. Tilt angle to minimise variability

This section offers an overview of the optimal tilt angles that minimise energy output variability across three different time resolutions: hourly, daily, and monthly. This analysis is based on an 11-year study period, where daily and monthly metrics represent the total aggregate generation over the respective intervals. An hourly temporal resolution is considered most appropriate to minimise real-time variability at both sites and reduce balancing costs, as electricity is commonly traded for each hour individually in the day-ahead market [99]. In power system modelling, this resolution is relatively coarse, as more granular resolutions, such as 5 to 15 min, are commonly used. Previous studies suggest that higher temporal resolutions more accurately capture the variability inherent in renewable energy generation [100]. For these reasons, of the three-time intervals considered in this work, the hourly analysis may be expected to offer the most relevant insights for a hybrid farm which exports directly to an electrical grid. Obviously, the hourly variability is

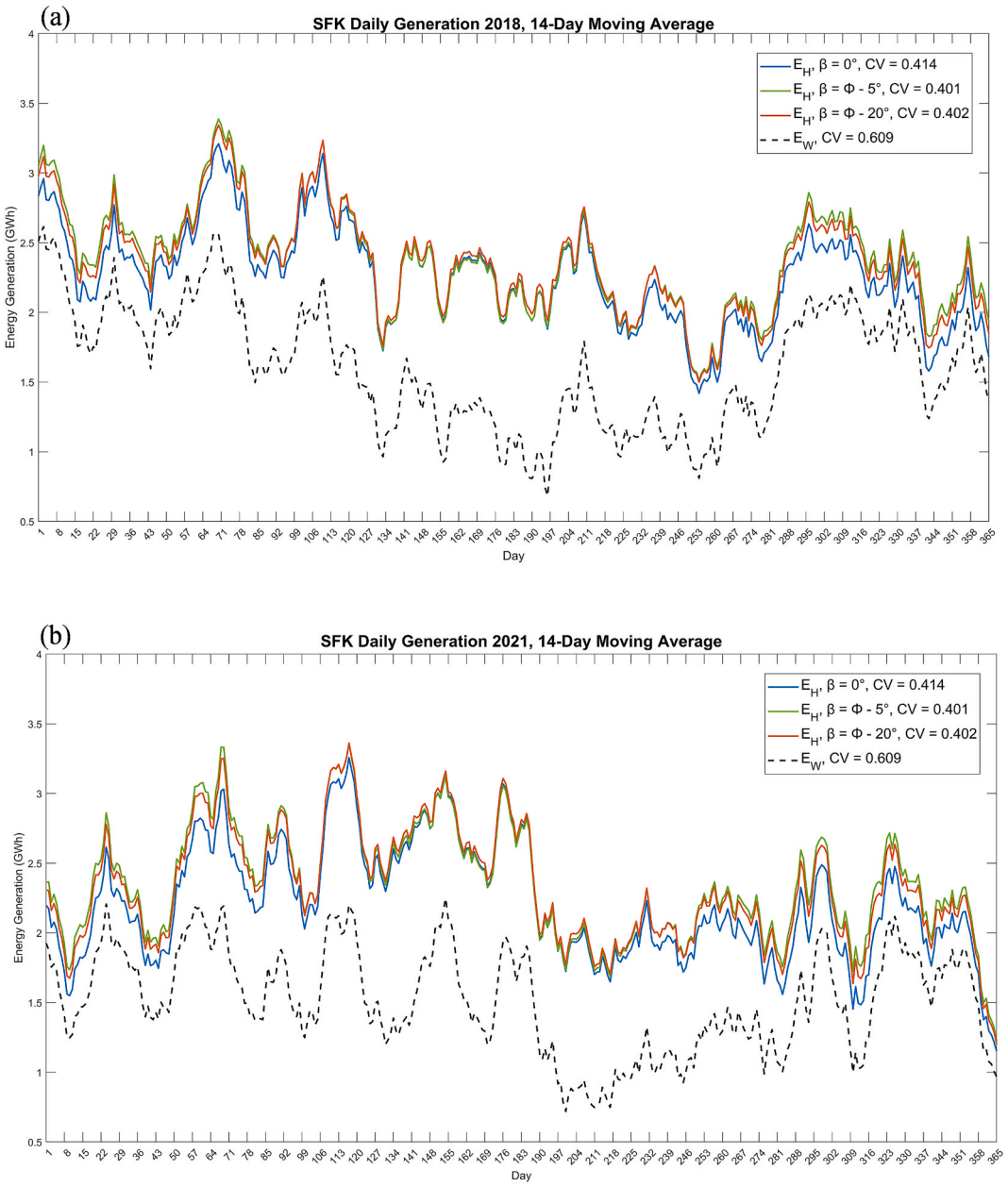


Fig. 11. Coefficient of variation of the hybrid site energy generation and wind-only energy generation for three tilt angles at SFK: (a) daily, 2018; (b) daily, 2021.

significantly affected by the day-night cycle of sunlight. The variation of the total daily hybrid energy generation is less influenced by the day-night cycle and can help capture weather pattern affects which typically have a persistence of many days in Europe and the North Atlantic [101]. The monthly hybrid electricity generation differs by season, accounting for seasonal shifts while reducing the noise of daily fluctuations [102]. The long-term performance trend revealed by this monthly analysis should show how different tilt angles affect year-round hybrid generation, particularly highlighting any "smoothing" effects throughout the year when compared to a wind-only scenario.

4.3.1. Hourly analysis

The data on an hourly time scale (Fig. 6) indicate that a tilt angle $\beta = 0\ ^\circ$ (horizontal solar panels) is the optimum for achieving the lowest energy variability. For larger values of the tilt angle, the CV increases, for both SFK and WMR.

The results can be visualised in Fig. 7 (a) (b) (c) and Fig. 8 (a) (b) (c), which show the hourly hybrid and stand-alone energy generation over five-day periods during the winter solstice, March equinox and summer solstice at WMR and SFK. To diminish the possibility of the selected period being a meteorological anomaly, data from three different years were presented adjacent to each other. To enhance visual clarity, only four scenarios were shown: the hybrid generation for $\beta = 0^\circ$, $\beta = \phi - 5^\circ$ and $\beta = \phi - 20^\circ$, and the wind-only energy generation.

Consistent with the previous calculations, a horizontally deployed solar PV system demonstrates minimal variation in energy output, irrespective of the season, year, or geographical location. This effect can be explained by the diurnal pattern of solar energy generation and the fact that tilted panels produce more energy relative to horizontal panels in a synchronised manner (with synchronous peaks). Tilted solar PV systems exhibit more amplified energy peaks relative to horizontal panels, which leads to a more variable energy output. In other words, inclined PV panels produce more energy than horizontal PV panels at the expense of greater variation.

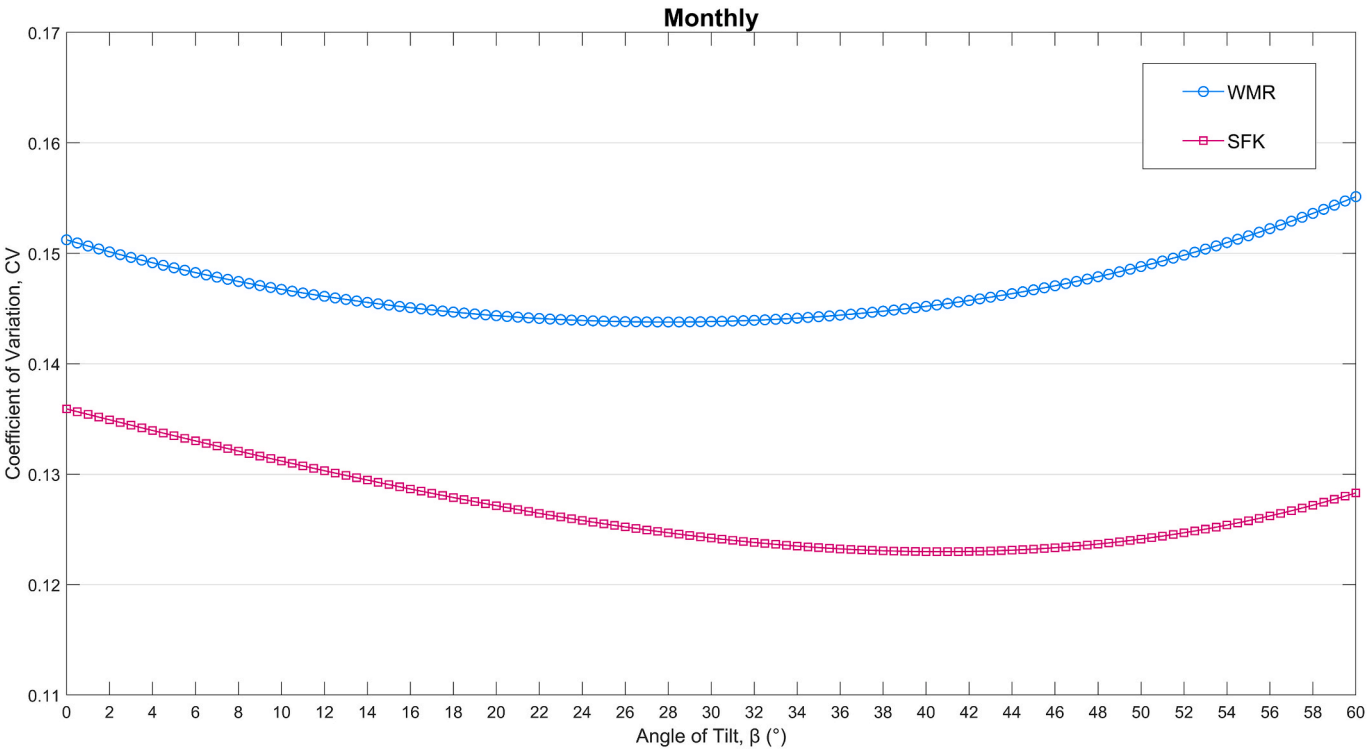


Fig. 12. Hybrid energy coefficient of variation of the hybrid farms for different tilt angles across the 11-year study period, calculated on a monthly timescale.

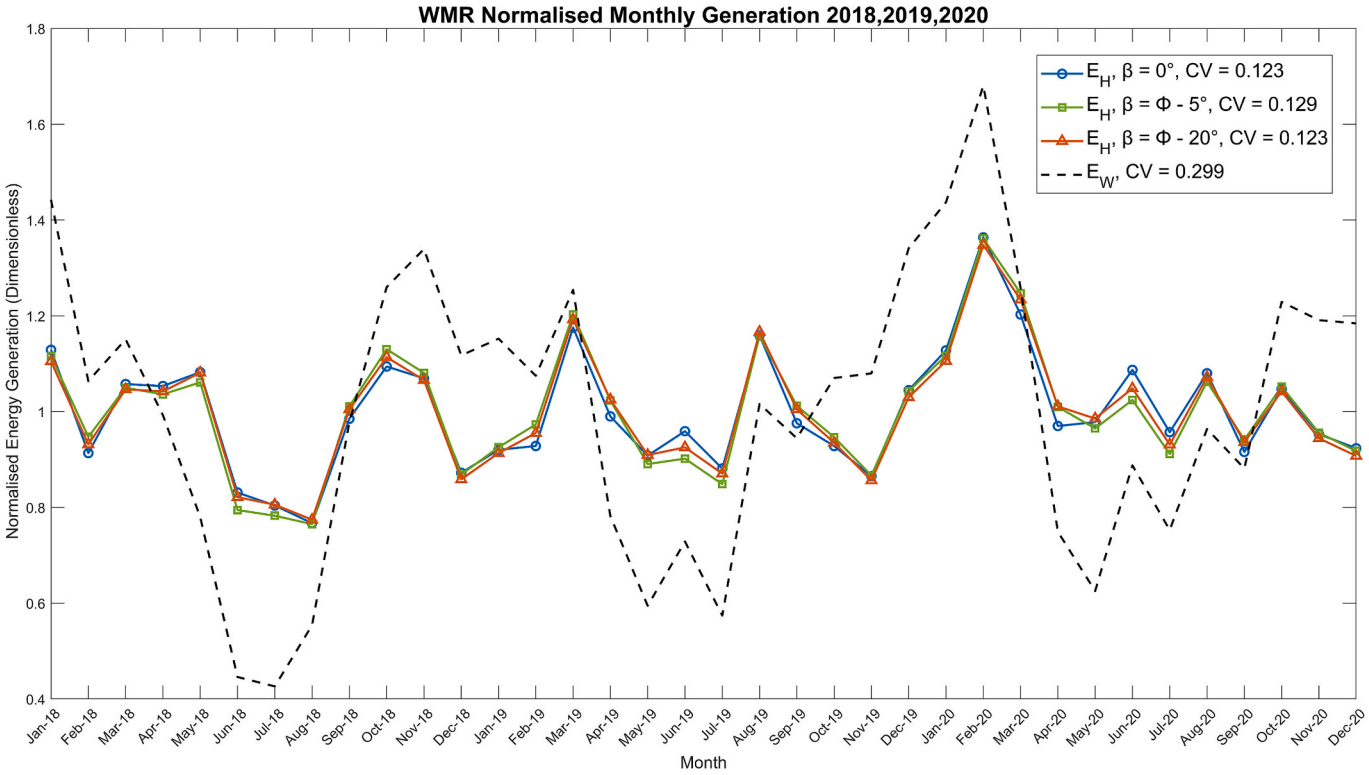


Fig. 13. Coefficient of variation of the hybrid site normalised energy generation and wind-only energy generation for three tilt angles at WMR on a monthly scale for 2018, 2019 and 2020.

4.3.2. Daily & monthly analysis

The analysis conducted on a daily time scale reveals significantly different results. Fig. 9 illustrates how the level of variability follows an almost "U-shaped" pattern, with the angle of tilt, β. The minimum CV occurs at an angle of tilt of 32.5° ($\phi-$ 8.5°) for SFK and 38.5° ($\phi-$ 15.3°) for WMR, as displayed in Table 7. This table presents the tilt angles that resulted in the lowest energy output variation across all three timescales, along with the angles that achieved the highest energy output over the

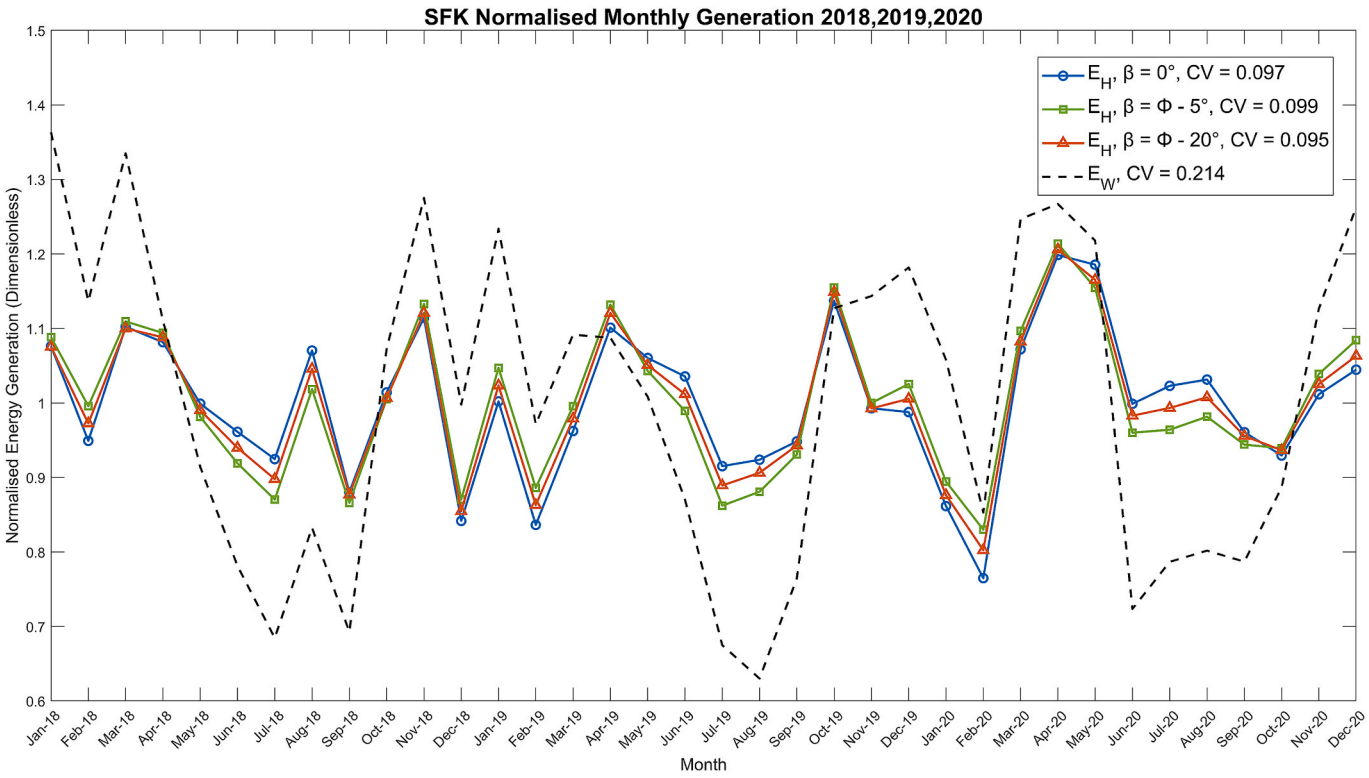


Fig. 14. Coefficient of variation of the hybrid site normalised energy generation and wind-only energy generation for three tilt angles at SFK on a monthly scale for 2018, 2019 and 2020.

11-year study period. In addition, Table 8 shows the lowest CV values obtained and the corresponding tilt angle for achieving this CV, as well as the wind-only energy output variation.

These findings can be demonstrated in Fig. 10 for WMR and Fig. 11 for SFK which display the daily generation across 2018 and 2021. The graph shows a 14-day moving average of the original (raw) time series for clarity, with the raw data used for the CV calculation. Both farms experience significantly lower wind generation during the summer months, which is effectively complemented by solar generation, regardless of tilt angle, as solar output is higher in summer.

Importantly, the integration of a horizontal PV system at the WMR wind farm reduces the CV from 0.713 for wind-only generation to 0.476 in 2018. Similarly, for the same year at SFK, the CV reduced from 0.609 for wind-only generation to 0.414 for hybrid generation with a tilt angle of 0°. For both sites, increasing the tilt angle led to smaller reductions in variability compared to the un-titled scenario.

Shifting the focus to a monthly temporal resolution, the analysis further supports the proposal of tilting the PV system off the horizontal plane to reduce variability and increase the energy yield at both sites. As depicted in Fig. 12 and Table 7, the tilt angle to achieve the lowest level of variation is 40.5° ($\phi - 0.5^{\circ}$) for SFK and 28° ($\phi - 25.8^{\circ}$) for WMR. At these angles, the coefficient of variation (CV) decreases to 0.123 from 0.136 for SFK and to 0.144 from 0.151 for WMR when the system is un-tilted. Figs. 13 and 14 show the normalised monthly energy generation for 2018–2020 at the SFK and WMR sites, with each profile normalised against the three-year average generation at the respective site. The hybrid configurations with PV tilt reduce inter-month variability, as indicated by the smaller dispersion of normalised values around the mean.

4.4. Correlation analysis

The angle of tilt influences the correlation between wind and solar generation, as measured by Pearson's r and Kendall's τ. At WMR, τ decreases slightly and linearly from − 0.0019 at β = 0° to − 0.003 at β = 60° in the hourly analysis, while r increases linearly from − 0.183 to − 0.142 (Fig. 15). A similar pattern is observed at SFK (Fig. 16), where τ declines marginally from − 0.0033 to − 0.0035 and r rises from − 0.122 to − 0.108.

On the daily scale, both correlation measures increase with tilt angle at each site, indicating a shift toward less negative correlation. At WMR, τ increases from − 0.254 to − 0.217 and r from − 0.378 to − 0.322 between β = 0° and 60°. At SFK, τ rises from − 0.143 to − 0.091, while r increases from − 0.211 to − 0.148 over the same range. This reflects a clearer reduction in complementarity compared to the hourly results.

The same trend persists on the monthly scale, where the strongest changes are observed. At WMR, τ increases from − 0.586 to − 0.551 and r from − 0.786 to − 0.754 as tilt increases from 0° to 60°. At SFK, τ rises from − 0.329 to − 0.292, while r increases from − 0.514 to − 0.420. These increases in both τ and r indicate that wind and solar generation become more synchronised at higher tilt angles. This reduction in complementarity at the monthly scale can be explained by seasonal effects. Higher tilt angles enhance solar generation during winter months, when solar elevation is lower. As winter also corresponds to periods of stronger wind generation, this leads to increased temporal alignment between the two resources, and consequently higher (i.e., less negative) correlation values.

4.5. Impact on energy yield

As observed, the tilt angle has a notable effect on the energy generation of the FPV system. As shown in Table 7 and Fig. 13, the maximum achievable hybrid farm capacity factor ($CF_{H,max}$) is 32.33% for SFK and 27.98% for WMR. This corresponds to an annual energy production (AEP_H) of 1,185 GWh for WMR and 860.5 GWh for SFK. For an un-tilted FPV system, the hourly hybrid energy output variability is minimised; however, overall energy generation is also reduced. On average, this configuration results in an annual loss of 46.2 GWh and

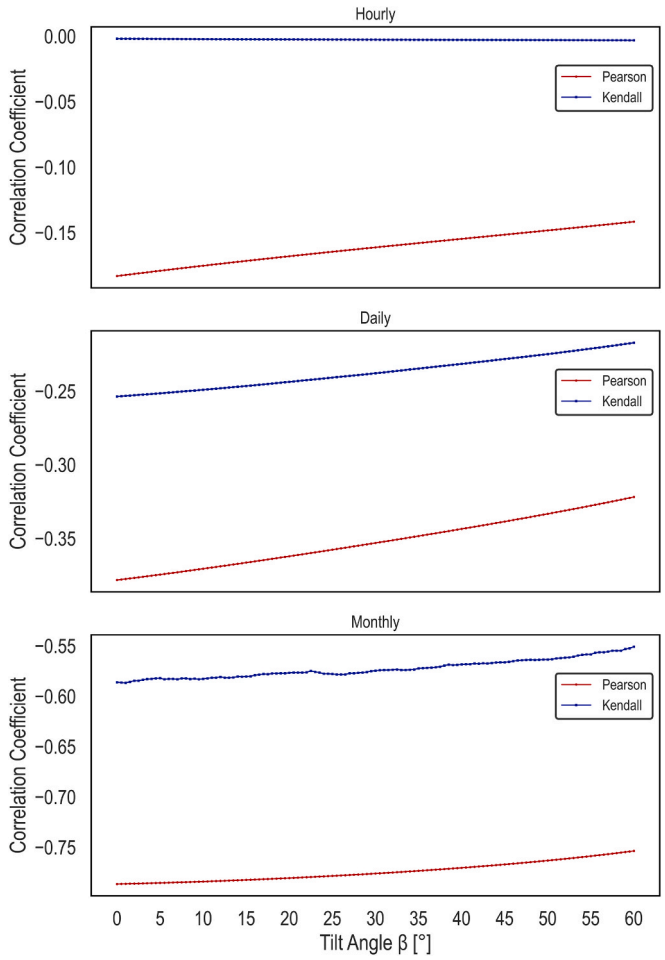


Fig. 15. Pearson's and Kendall's correlation coefficients between wind and solar generation for different tilt angles over the 11-year study period at WMR, calculated at hourly, daily, and monthly timescales.

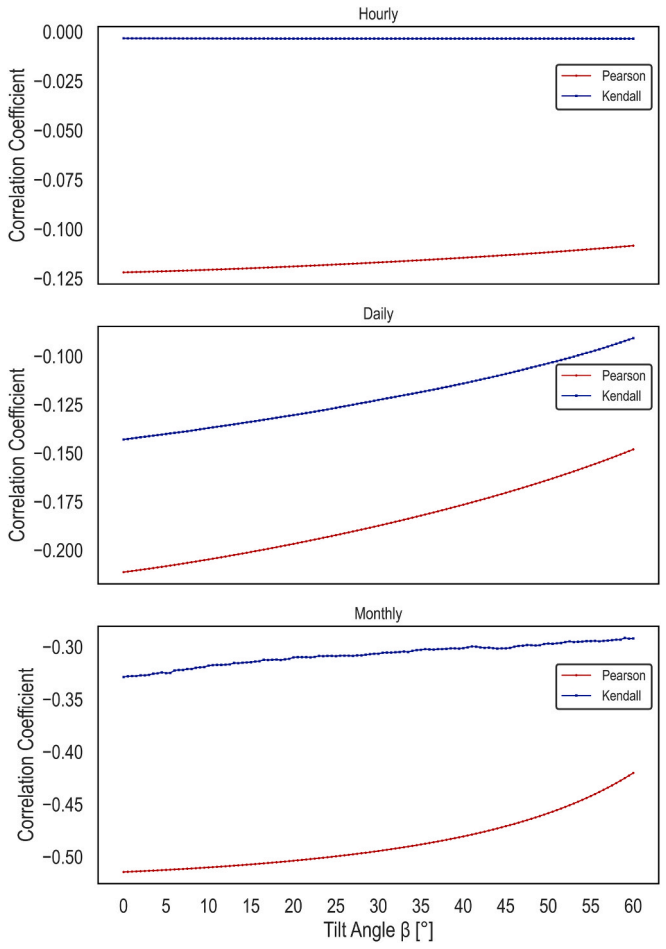


Fig. 16. Pearson's and Kendall's correlation coefficients between wind and solar generation for different tilt angles over the 11-year study period at SFK, calculated at hourly, daily, and monthly timescales.

81.8 GWh of potential solar energy for SFK and WMR, respectively. When tilted at the angle that minimises daily energy variation, denoted as $\beta\{CV_{min}^{(d)}\}$, the annual loss of potential solar energy is significantly reduced to just 0.54 GWh for SFK and 1.45 GWh for WMR, bringing the system's output much closer to its maximum potential. Likewise, when optimised for monthly energy variation with $\beta\{CV_{min}^{(m)}\}$, the losses are reduced to 0.675 GWh for SFK and 11.64 GWh for WMR. These findings show that variability can be reduced while simultaneously increasing energy generation.

Fig. 17 illustrates how the potential energy yield is influenced by the angle of tilt, highlighting the specific tilt angles that were found to reduce variability on hourly, daily, and monthly timescales and the tilt angle to achieve $CF_{H,max}$.

5. Conclusions

This study evaluates the impact of the tilt angle of the floating photovoltaic (FPV) subsystem of a hybrid offshore wind – solar PV farm on the variability of its power output. The underlying concept is the hybridisation of existing offshore wind farms by retrofitting them with solar PV energy. Notwithstanding, another possibility would be the installation of hybrid offshore wind – solar PV farms *ex novo*.

Two case studies are considered deployed for the retrofitting – South Fork Wind Farm (USA) and Westermost Rough Wind Farm (UK) – with the primary aim of reducing the variability of their power output. The specific objective is to investigate whether, and if so, how changes in the tilt angle of the PV subsystem influence the variability at these two locations.

Hourly wind speed data were vertically extrapolated to the wind farm hub height using the power law, and the power output was subsequently calculated based on the corresponding power curves. For solar energy, horizontal diffuse and direct irradiance were translated to the tilted plane using the Hay–Davies–Klucher–Reindl method. Calculations were performed for tilt angles ranging from 0° to 60° in 0.5° increments. A typical monocrystalline photovoltaic module was selected for the hypothetical solar installations. Informed by previous studies aimed at minimising energy variability, the solar-to-wind installation capacity ratio was set at a constant ratio of 1.3:1 throughout the study. The coefficient of variation was the metric selected to express the variability of combined wind and solar energy generation from the study sites. The analysis was performed across three timescales: hourly, daily, and monthly.

The following conclusions may be drawn. First, a horizontal deployment of the solar panels (tilt angle of 0°) minimises the hourly variability of the energy output of the hybrid farm (relative to the existing, non-hybrid wind farms) significantly: by 15.6% and 19.5% at South Fork and Westermost Rough, respectively. However, this reduction in variability comes at the expense of slightly lower hybrid capacity factors: 30.6% at South Fork and 26.04% at Westermost Rough. For comparison, the maximum possible hybrid capacity factors, 32.3% and 27.98%, correspond to tilt angles of 35.5° and 43.5° at South Fork and Westermost Rough, respectively. Second, on a daily timescale, the variability decreased by 34.4% for SFK and 35.7% for WMR when the tilt angles were set to 32.5° and 38.5°, respectively. The tilted solar modules

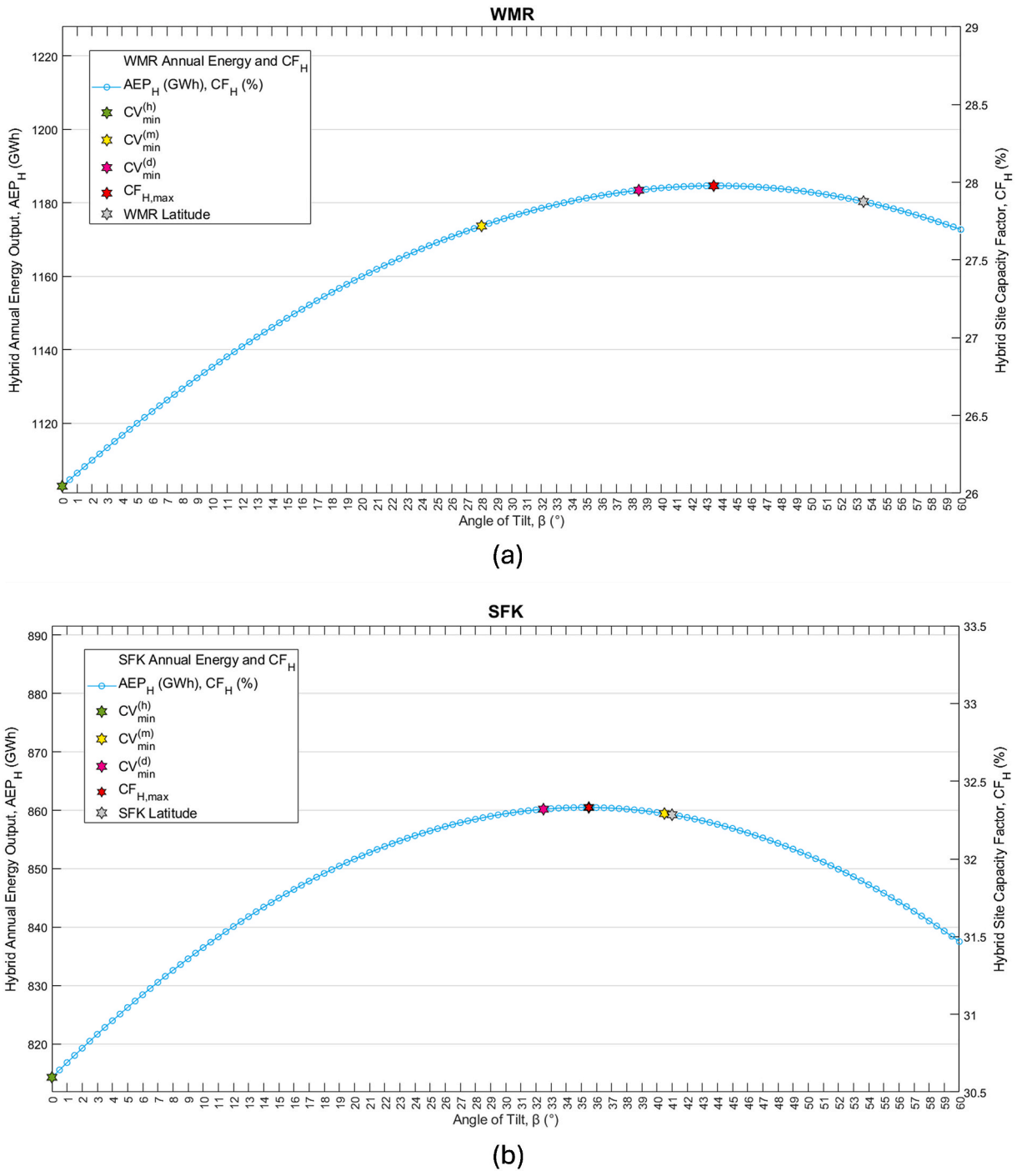


Fig. 17. Hybrid farm annual energy production (AEP, left-hand vertical axis) and capacity factor (CF_H, right-hand vertical axis) as a function of the angle of tilt of the solar PV panels for the (a) WMR and (b) SFK farms. The angles corresponding to the maximum capacity factor and annual energy production ($CF_{H,max}$), and to the minimum values of the coefficient of variation at hourly ($CV_{min}^{(h)}$), daily ($CV_{min}^{(d)}$), and monthly ($CV_{min}^{(d)}$) timescales are indicated by the coloured stars, as is the latitude of the site.

captured more energy, which increased the hybrid site capacity factors to 32.2% for SFK and 27.95% for WMR. This demonstrates that energy generation can be enhanced while minimising variability by retrofitting offshore wind farms with tilted solar PV systems.

Third, the variability of the power output was decreased by 42.9% at SFK and 56.3% at WMR for tilt angles of 40.5° and 28°, respectively when the analysis was carried out on the monthly timescale. Importantly, the installation of a floating photovoltaic (FPV) system, regardless of tilt angle, significantly reduced the variability of the energy output of the hybrid farm compared to a conventional (stand-alone wind) farm across all timescales.

Across the three timescales considered, the optimal tilt angle for minimising variability and maximising energy yield varied. Therefore, in practice the strategy should depend on the specific objectives for mitigation of variability at the level of the electricity grid operator.

Adjusting the tilt angle in a hybrid farm was proven to damp the variability, and more generally, the hybridisation of existing wind farms was shown to be a promising option not least because of this damping. However, this investigation, at the level of the hybrid farm, must be complemented by future work at the level of the entire electricity grid.

CRediT authorship contribution statement

Josh Moore: Writing – original draft, Visualization, Validation, Software, Resources, Methodology, Investigation, Formal analysis, Data curation, Conceptualization. **Gregorio Iglesias:** Writing – review & editing, Supervision, Resources, Project administration, Methodology, Funding acquisition, Conceptualization.

Declaration of competing interest

The authors declare that they have no known competing financial interests or personal relationships that could have appeared to influence the work reported in this paper.

Acknowledgements

This work was partially supported by the European Union's Horizon 2020 Programme (H2020-LC-GD-20204), grants No. 101037643 – ILIAD and 101129716 - LITEFLOATCON.

The authors are thankful to the European Centre for Medium-Range Weather Forecasts (ECMWF) within the Copernicus programme, which provides the ERA5 reanalysis data used in this work. Data is publicly available through the Copernicus Climate Data Store (CDS), https://cds.climate.copernicus.eu/datasets.

Data availability

Data will be made available on request.

References

[1] Dang DA, La HA. Does electricity reliability matter? Evidence from rural Viet Nam. Energy Policy Aug. 2019;131:399–409. https://doi.org/10.1016/j.enpol.2019.04.036.
[2] Alex, 'Global Offshore Wind Report 2023', Global Wind Energy Council. Accessed: Jan. 15, 2025. [Online]. Available: https://gwec.net/gwecs-global-offshore-wind-report-2023/.
[3] B. Backwell *et al.*, 'GWEC-Global-Offshore-Wind-Report-2024', 2024.
[4] Rubio-Domingo G, Linares P. The future investment costs of offshore wind: an estimation based on auction results. Renew Sustain Energy Rev Sep. 2021;148:111324. https://doi.org/10.1016/j.rser.2021.111324.
[5] Bilgili M, Yasar A, Simsek E. Offshore wind power development in Europe and its comparison with onshore counterpart. Renew Sustain Energy Rev Feb. 2011;15(2):905–15. https://doi.org/10.1016/j.rser.2010.11.006.
[6] Henderson AR, Morgan C, Smith B, Sørensen HC, Barthelmie RJ, Boesmans B. Offshore Wind Energy in Europe— a Review of the State-of-the-Art. Wind Energy 2003;6(1):35–52. https://doi.org/10.1002/we.82.
[7] S. Tumse, M. Bilgili, A. Yildirim, and B. Sahin, 'Comparative Analysis of Global Onshore and Offshore Wind Energy Characteristics and Potentials', *Sustainability*, vol. 16, no. 15, Art. no. 15, Jan. 2024, doi: 10.3390/su16156614.
[8] Desalegn B, Gebeyehu D, Tamrat B, Tadiwose T, Lata A. Onshore versus offshore wind power trends and recent study practices in modeling of wind turbines' life-cycle impact assessments. Clean Eng Technol Dec. 2023;17:100691. https://doi.org/10.1016/j.clet.2023.100691.
[9] Astariz S, Iglesias G. The collocation feasibility index – a method for selecting sites for co-located wave and wind farms. Renew Energy Apr. 2017;103:811–24. https://doi.org/10.1016/j.renene.2016.11.014.
[10] Huang J, Iglesias G. Hybrid offshore wind–solar energy farms: a novel approach through retrofitting. Energy Convers Manag Nov. 2024;319:118903. https://doi.org/10.1016/j.enconman.2024.118903.
[11] Martinez A, Iglesias G. Hybrid wind-solar energy resources mapping in the European Atlantic. Sci Total Environ Jun. 2024;928:172501. https://doi.org/10.1016/j.scitotenv.2024.172501.
[12] X. Costoya, M. deCastro, D. Carvalho, B. Arguilé-Pérez, and M. Gómez-Gesteira, 'Combining offshore wind and solar photovoltaic energy to stabilize energy supply under climate change scenarios: A case study on the western Iberian Peninsula', *Renew. Sustain. Energy Rev.*, vol. 157, p. 112037, Apr. 2022, doi: 10.1016/j.rser.2021.112037.
[13] M. M. De Souza Nascimento, M. Shadman, C. Silva, L. P. De Freitas Assad, S. F. Estefen, and L. Landau, 'Offshore wind and solar complementarity in Brazil: A theoretical and technical potential assessment', *Energy Convers. Manag.*, vol. 270, p. 116194, Oct. 2022, doi: 10.1016/j.enconman.2022.116194.
[14] Pérez-Collazo C, Greaves D, Iglesias G. A review of combined wave and offshore wind energy. Renew Sustain Energy Rev Feb. 2015;42:141–53. https://doi.org/10.1016/j.rser.2014.09.032.
[15] Astariz S, Iglesias G. Output power smoothing and reduced downtime period by combined wind and wave energy farms. Energy Feb. 2016;97:69–81. https://doi.org/10.1016/j.energy.2015.12.108.
[16] Gaughan E, Fitzgerald B. An assessment of the potential for Co-located offshore wind and wave farms in Ireland. Energy Jun. 2020;200:117526. https://doi.org/10.1016/j.energy.2020.117526.
[17] I. CORPORATIVA, 'Iberdrola, present in Australia with the world's first wind-solar hybrid plant', Iberdrola. Accessed: Mar. 06, 2025. [Online]. Available: https://www.iberdrola.com/about-us/what-we-do/onshore-wind-energy/port-augusta-project.
[18] Frade PMS, Pereira JP, Santana JJE, Catalão JPS. Wind balancing costs in a power system with high wind penetration – evidence from Portugal. Energy Policy Sep. 2019;132:702–13. https://doi.org/10.1016/j.enpol.2019.06.006.
[19] 'EWEA-position-paper-balancing-responsibility-and-costs.pdf'. Accessed: Feb. 27, 2025. [Online]. Available: https://windeurope.org/fileadmin/files/library/publications/position-papers/EWEA-position-paper-balancing-responsibility-and-costs.pdf.
[20] Reikard G, Robertson B, Bidlot J-R. Combining wave energy with wind and solar: short-term forecasting. Renew Energy Sep. 2015;81:442–56. https://doi.org/10.1016/j.renene.2015.03.032.
[21] N. Skopljak, 'Floating solar market will be as big as onshore solar sector, says Oceans of Energy CEO', Offshore Energy. Accessed: Feb. 27, 2025. [Online]. Available: https://www.offshore-energy.biz/floating-solar-market-will-be-as-big-as-onshore-solar-sector-says-oceans-of-energy-ceo/.
[22] Martinez A, Iglesias G. 'Levelized cost of energy to evaluate the economic viability of floating offshore wind in the European Atlantic and Mediterranean', *E-Prime - Adv.* Electr Eng Electron Energy Jun. 2024;8:100562. https://doi.org/10.1016/j.prime.2024.100562.
[23] B. Thomas, X. Costoya, M. deCastro, G. Iglesias, and M. Gómez-Gesteira, 'Levelized cost of energy for various floating offshore wind farm designs in the areas covered by the Spanish maritime spatial planning', *Appl. Energy*, vol. 381, p. 125165, Mar. 2025, doi: 10.1016/j.apenergy.2024.125165.
[24] Astariz S, Vazquez A, Sánchez M, Carballo R, Iglesias G. Co-located wave-wind farms for improved O&M efficiency. Ocean Coast Manag Sep. 2018;163:66–71. https://doi.org/10.1016/j.ocecoaman.2018.04.010.
[25] Pringle AM, Handler RM, Pearce JM. Aquavoltaics: Synergies for dual use of water area for solar photovoltaic electricity generation and aquaculture. Renew Sustain Energy Rev Dec. 2017;80:572–84. https://doi.org/10.1016/j.rser.2017.05.191.
[26] Canul-Reyes DA, Rodríguez-Hernández O, Barragán-Peña ME, Del Rio JA. Analysis of offshore wind energy and solar photovoltaic production and its relationship with regional electricity demand in the Yucatan peninsula. Energy Jan. 2025;314:134060. https://doi.org/10.1016/j.energy.2024.134060.
[27] Li P, Lian J, Ma C, Zhang J. Complementarity and development potential assessment of offshore wind and solar resources in China seas. Energy Convers Manag Nov. 2023;296:117705. https://doi.org/10.1016/j.enconman.2023.117705.
[28] W. Hou, X. Zhang, M. Wu, Yuxin Feng, and L. Yang, 'Integrating stability and complementarity to assess the accommodable generation potential of multiscale solar and wind resources: A case study in a resource-based area in China', *Energy*, vol. 261, p. 125312, Dec. 2022, doi: 10.1016/j.energy.2022.125312.
[29] Schindler D, Behr HD, Jung C. On the spatiotemporal variability and potential of complementarity of wind and solar resources. Energy Convers Manag Aug. 2020;218:113016. https://doi.org/10.1016/j.enconman.2020.113016.
[30] Xu H, Zhang J, Cheng C, Cao H, Lu J, Zhang Z. A novel metric for evaluating hydro-wind-solar energy complementarity. Appl Energy Nov. 2024;373:123926. https://doi.org/10.1016/j.apenergy.2024.123926.
[31] Hajou A, El Mghouchi Y, Chaoui M. A new solar-wind complementarity index: an application to the climate of Morocco. Renew Energy Jun. 2024;227:120490. https://doi.org/10.1016/j.renene.2024.120490.
[32] Xu L, Wang Z, Liu Y. The spatial and temporal variation features of wind-sun complementarity in China. Energy Convers Manag Dec. 2017;154:138–48. https://doi.org/10.1016/j.enconman.2017.10.031.
[33] Magaña-González RC, Rodríguez-Hernández O, Canul-Reyes DA. Analysis of seasonal variability and complementarity of wind and solar resources in Mexico. Sustain Energy Technol Assess Dec. 2023;60:103456. https://doi.org/10.1016/j.seta.2023.103456.
[34] K. A. Folly and N. Makhubele, 'An Investigation into the Complementarity of Wind and Solar Resources: A Case Study', in *2024 32nd Southern African Universities Power Engineering Conference (SAUPEC)*, Stellenbosch, South Africa: IEEE, Jan. 2024, pp. 1–5. doi: 10.1109/SAUPEC60914.2024.10445090.
[35] Al-Shereiqi A, Al-Hinai A, Albadi M, Al-Abri R. Optimal Sizing of Hybrid Wind-Solar Power Systems to Suppress output fluctuation. Energies Aug. 2021;14(17):5377. https://doi.org/10.3390/en14175377.
[36] Bakirci K. General models for optimum tilt angles of solar panels: Turkey case study. Renew Sustain Energy Rev Oct. 2012;16(8):6149–59. https://doi.org/10.1016/j.rser.2012.07.009.
[37] Rowlands IH, Kemery BP, Beausoleil-Morrison I. Optimal solar-PV tilt angle and azimuth: an Ontario (Canada) case-study. Energy Policy Mar. 2011;39(3):1397–409. https://doi.org/10.1016/j.enpol.2010.12.012.
[38] H. Z. Al Garni, A. Awasthi, and D. Wright, 'Optimal orientation angles for maximizing energy yield for solar PV in Saudi Arabia', *Renew. Energy*, vol. 133, pp. 538–550, Apr. 2019, doi: 10.1016/j.renene.2018.10.048.
[39] Abdeen E, Orabi M, Hasaneen E-S. Optimum tilt angle for photovoltaic system in desert environment. Sol Energy Oct. 2017;155:267–80. https://doi.org/10.1016/j.solener.2017.06.031.

[40] Shahriar K, Ali MH, Mahmud MK, Hossain MR. Optimization of combined electricity generation and cooling load reduction by incorporating roof top photovoltaic module: an approach to energy consumption reduction in a hospital building. Energy Convers Manag X Apr. 2025;26:100948. https://doi.org/10.1016/j.ecmx.2025.100948.
[41] Kapica J, Canales FA, Jurasz J. Global atlas of solar and wind resources temporal complementarity. Energy Convers Manag Oct. 2021;246:114692. https://doi.org/10.1016/j.enconman.2021.114692.
[42] J. Rakovec, K. Zaksek, K. Brecl, D. Kastelec, and M. Topic, 'Orientation and Tilt Dependence of a Fixed PV Array Energy Yield Based on Measurements of Solar Energy and Ground Albedo – a Case Study of Slovenia', in *Energy Management Systems*, G. Kini, Ed., InTech, 2011. doi: 10.5772/18386.
[43] 'PVGIS.COM - Solar Panel Tilt Angle Calculation: Complete Guide 2025'. Accessed: Mar. 18, 2026. [Online]. Available: https://pvgis.com/en/blog/solar-panel-tilt-angle-calculation.
[44] T. M. Yunus Khan *et al.*, 'Optimum location and influence of tilt angle on performance of solar PV panels', *J. Therm. Anal. Calorim.*, vol. 141, no. 1, pp. 511–532, Jul. 2020, doi: 10.1007/s10973-019-09089-5.
[45] A. M. Ali Morad, A. K. Shaker Al-Sayyab, and M. A. Abdulwahid, 'Optimisation of tilted angles of a photovoltaic cell to determine the maximum generated electric power: A case study of some Iraqi cities', *Case Stud. Therm. Eng.*, vol. 12, pp. 484–488, Sep. 2018, doi: 10.1016/j.csite.2018.07.001.
[46] Chung P-H, Chou C-C, Yang R-Y, Chung C-Y. Wind Loads on a PV Array. Appl Sci Jun. 2019;9(12):2466. https://doi.org/10.3390/app9122466.
[47] Su K-C, Chung P-H, Yang R-Y. Numerical simulation of wind loads on an offshore PV panel: the effect of wave angle. J Mech Nov. 2020;37:53–62. https://doi.org/10.1093/jom/ufaa010.
[48] Chou C-C, Chung P-H, Yang R-Y. Wind Loads on a Solar Panel at High Tilt Angles. Appl Sci Apr. 2019;9(8):1594. https://doi.org/10.3390/app9081594.
[49] '2014_02_26_wmr_pim_final_0.pdf'. Accessed: Jan. 20, 2025. [Online]. Available: https://www.ofgem.gov.uk/sites/default/files/docs/2014/02/2014_02_26_wmr_pim_final_0.pdf.
[50] 'Ground breaking Westermost Rough offshore wind farm is declared open'. Accessed: Jan. 29, 2025. [Online]. Available: https://orsted.co.uk/media/newsroom/news/2015/07/ground-breaking-westermost-rough-offshore-wind-farm-is-declared-open.
[51] Wędzik A, Szypowski M, Siewierski T. An integrated method to simultaneously optimise a wind farm's internal network layout, cable cross-sections and substation location. Appl Energy Jan. 2025;377:124361. https://doi.org/10.1016/j.apenergy.2024.124361.
[52] 'Westermost Rough (WMR) Offshore Wind Power Project, Yorkshire', Energy Monitor. Accessed: Jan. 29, 2025. [Online]. Available: https://www.energymonitor.ai/projects/westermost-rough-wmr-offshore-wind-power-project-yorkshire/.
[53] 'Westermost Rough Offshore Wind Farm - Fully Commissioned - United Kingdom | 4C Offshore'. Accessed: Jan. 29, 2025. [Online]. Available: https://www.4coffshore.com/windfarms/united-kingdom/westermost-rough-united-kingdom-uk34.html.
[54] 'UK: offshore wind capacity 2023', Statista. Accessed: Mar. 03, 2025. [Online]. Available: https://www.statista.com/statistics/792374/cumulative-offshore-wind-capacity-united-kingdom/.
[55] Shields M, et al. 'A Supply Chain Road Map for Offshore Wind Energy in the United States', National Renewable Energy Laboratory (NREL). Golden, CO (united States), NREL/TP-5000-84710, Jan 2023. https://doi.org/10.2172/1922189.
[56] 'South Fork Offshore Wind Farm | Project Details'. Accessed: Jan. 29, 2025. [Online]. Available: https://www.blackridgeresearch.com/project-profiles/south-fork-offshore-wind-farm-mill-power-plant-project-united-states-us-new-york-america-details.
[57] 'Powering up the Empire State with clean energy from the South Fork Wind farm'. Accessed: Jan. 29, 2025. [Online]. Available: https://southforkwind.com/about-south-fork-wind.
[58] R. Wiser, M. Hand, J. Seel, and B. Paulos, 'Reducing Wind Energy Costs through Increased Turbine Size: Is the Sky the Limit?'.
[59] '12. Offshore Foundations.pdf'. Accessed: Jan. 21, 2025. [Online]. Available: https://steelinfo.dk/files/pdf/dsi/Steelday_2014/12.%20Offshore%20Foundations.pdf.
[60] 'Full power at Westermost Rough offshore wind farm'. Accessed: Jan. 21, 2025. [Online]. Available: https://orsted.co.uk/media/newsroom/news/2015/05/full-power-at-westermost-rough-offshore-wind-farm.
[61] 'Westermost Rough Windfarm - Power-Station-Dictionary'. Accessed: Jan. 21, 2025. [Online]. Available: https://osuked.github.io/Power-Station-Dictionary/objects/10248.html#downloads.
[62] 'South Fork Offshore Substation', Kiewit Corporation. Accessed: Jan. 29, 2025. [Online]. Available: https://www.kiewit.com/projects/south-fork-offshore-substation/.
[63] D. Proctor, 'South Fork: A Positive Turn for U.S. Offshore Wind', POWER Magazine. Accessed: Jan. 29, 2025. [Online]. Available: https://www.powermag.com/south-fork-a-positive-turn-for-u-s-offshore-wind/.
[64] 'Siemens SWT-6.0-154 - Manufacturers and turbines - Online access - The Wind Power'. Accessed: Jan. 21, 2025. [Online]. Available: https://www.thewindpower.net/turbine_en_807_siemens_swt-6.0-154.php.
[65] 'Siemens D6 platform – 6.0-MW direct drive wind turbine'. Accessed: Mar. 29, 2026. [Online]. Available: https://assets.new.siemens.com/siemens/assets/api/uuid:1c690d9444b15f1a542d0e3166f43a90814743f2/d6-offshore-brochure-en.pdf.
[66] L. Bauer, 'Siemens Gamesa SG 11.0-200 DD - 11,00 MW - Wind turbine'. Accessed: Jan. 29, 2025. [Online]. Available: https://en.wind-turbine-models.com/turbines/2157-siemens-gamesa-sg-11.0-200-dd.
[67] 'Vestas V164/9500 - Manufacturers and turbines - Online access - The Wind Power'. Accessed: Feb. 12, 2025. [Online]. Available: https://www.thewindpower.net/turbine_en_1476_vestas_v164-9500.php.
[68] 'Catalogue — Climate Data Store'. Accessed: Mar. 19, 2025. [Online]. Available: https://cds.climate.copernicus.eu/datasets.
[69] 'Optimization of tilt angle for PV in China with long-term hourly surface solar radiation - ScienceDirect'. Accessed: Feb. 17, 2025. [Online]. Available: https://www.sciencedirect.com/science/article/pii/S0960148124008097.
[70] J. Jurasz, J. Mikulik, P. B. Dąbek, M. Guezgouz, and B. Kaźmierczak, 'Complementarity and "Resource Droughts" of Solar and Wind Energy in Poland: An ERA5-Based Analysis', *Energies*, vol. 14, no. 4, Art. no. 4, Jan. 2021, doi: 10.3390/en14041118.
[71] Hayes L, Stocks M, Blakers A. Accurate long-term power generation model for offshore wind farms in Europe using ERA5 reanalysis. Energy Aug. 2021;229:120603. https://doi.org/10.1016/j.energy.2021.120603.
[72] Mathews D, Gallachóir BÓ, Deane P. Systematic bias in reanalysis-derived solar power profiles & the potential for error propagation in long duration energy storage studies. Appl Energy Apr. 2023;336:120819. https://doi.org/10.1016/j.apenergy.2023.120819.
[73] 'ERA5 hourly data on single levels from 1940 to present'. Accessed: Feb. 18, 2025. [Online]. Available: https://cds.climate.copernicus.eu/datasets/reanalysis-era5-single-levels?tab=overview.
[74] 'Solar', IEA. Accessed: Feb. 17, 2025. [Online]. Available: https://www.iea.org/energy-system/renewables/solar-pv.
[75] Y. Sawle and M. Thirunavukkarasu, 'Chapter 9 - Techno-economic comparative assessment of an off-grid hybrid renewable energy system for electrification of remote area', in *Design, Analysis, and Applications of Renewable Energy Systems*, A. T. Azar and N. A. Kamal, Eds, in Advances in Nonlinear Dynamics and Chaos (ANDC). , Academic Press, 2021, pp. 199–247. doi: 10.1016/B978-0-12-824555-2.00027-7.
[76] 'Monocrystalline solar panels: the expert guide [2025]'. Accessed: Feb. 17, 2025. [Online]. Available: https://www.sunsave.energy/solar-panels-advice/solar-technology/monocrystalline.
[77] 'EU_Datasheet_VertexS_DE09.08_2021_A.pdf'. Accessed: Feb. 18, 2025. [Online]. Available: https://static.trinasolar.com/sites/default/files/EU_Datasheet_VertexS_DE09.08_2021_A.pdf.
[78] Maatallah T, El Alimi S, Nassrallah SB. Performance modeling and investigation of fixed, single and dual-axis tracking photovoltaic panel in Monastir city, Tunisia. Renew Sustain Energy Rev Oct. 2011;15(8):4053–66. https://doi.org/10.1016/j.rser.2011.07.037.
[79] Xu R, Ni K, Hu Y, Si J, Wen H, Yu D. Analysis of the optimum tilt angle for a soiled PV panel. Energy Convers Manag Sep. 2017;148:100–9. https://doi.org/10.1016/j.enconman.2017.05.058.
[80] 'How HOMER Calculates the Radiation Incident on the PV Array'. Accessed: Jan. 28, 2025. [Online]. Available: https://homerenergy.com/products/pro/docs/3.15/how_homer_calculates_the_radiation_incident_on_the_pv_array.html.
[81] Kaddoura TO, Ramli MAM, Al-Turki YA. On the estimation of the optimum tilt angle of PV panel in Saudi Arabia. Renew Sustain Energy Rev Nov. 2016;65:626–34. https://doi.org/10.1016/j.rser.2016.07.032.
[82] C. Breyer and J. Schmid, 'GLOBAL DISTRIBUTION OF OPTIMAL TILT ANGLES FOR FIXED TILTED PV SYSTEMS'.
[83] M. S. Khan, M. A. M. Ramli, H. F. Sindi, T. Hidayat, and H. R. E. H. Bouchekara, 'Estimation of Solar Radiation on a PV Panel Surface with an Optimal Tilt Angle Using Electric Charged Particles Optimization', *Electronics*, vol. 11, no. 13, Art. no. 13, Jan. 2022, doi: 10.3390/electronics11132056.
[84] R. E. Payne, 'Albedo of the Sea Surface', Jul. 1972, Accessed: Jan. 28, 2025. [Online]. Available: https://journals.ametsoc.org/view/journals/atsc/29/5/1520-0469_1972_029_0959_aotss_{20}_co_2.xml.
[85] Canales FA, Jurasz J, Beluco A, Kies A. Assessing temporal complementarity between three variable energy sources through correlation and compromise programming. Energy Feb. 2020;192:116637. https://doi.org/10.1016/j.energy.2019.116637.
[86] A. Djalab, Z. Djalab, A. El Hammoumi, G. Marco TINA, S. Motahhir, and A. A. Laouid, 'A comprehensive Review of Floating Photovoltaic Systems: Tech Advances, Marine Environmental Influences on Offshore PV Systems, and Economic Feasibility Analysis', *Sol. Energy*, vol. 277, p. 112711, Jul. 2024, doi: 10.1016/j.solener.2024.112711.
[87] 'Prediction Model of Photovoltaic Module Temperature for Power Performance of Floating PVs'. Accessed: Jan. 28, 2025. [Online]. Available: https://www.mdpi.com/1996-1073/11/2/447.
[88] Fırtın E, Güler Ö, Akdağ SA. Investigation of wind shear coefficients and their effect on electrical energy generation. Appl Energy Nov. 2011;88(11):4097–105. https://doi.org/10.1016/j.apenergy.2011.05.025.
[89] 'Global offshore wind capacity factor 2023 | Statista'. Accessed: Feb. 19, 2025. [Online]. Available: https://www.statista.com/statistics/1368679/global-offshore-wind-capacity-factor/.
[90] 'Assessment of wind and wave power characteristic and potential for hybrid exploration in Australia - ScienceDirect'. Accessed: Feb. 20, 2025. [Online]. Available: https://www.sciencedirect.com/science/article/pii/S1364032122006347?casa_token=MQeZd4zDMPkAAAAA:LijF40mNNxiX8UXJRh9L2jGOsXKuA0Zqqw27jwStyu_r6OWvOyYG0ANIbMGKN2lUJ0-z876B.

[91] 'Combining offshore wind and solar photovoltaic energy to stabilize energy supply under climate change scenarios: A case study on the western Iberian Peninsula - ScienceDirect'. Accessed: Feb. 20, 2025. [Online]. Available: https://www.sciencedirect.com/science/article/pii/S1364032121012995.
[92] Soukissian TH, Karathanasi FE, Zaragkas DK. Exploiting offshore wind and solar resources in the Mediterranean using ERA5 reanalysis data. Energy Convers Manag Jun. 2021;237:114092. https://doi.org/10.1016/j.enconman.2021.114092.
[93] 'download.pdf'. Accessed: Feb. 20, 2025. [Online]. Available: https://www.neso.energy/document/318666/download.
[94] 'Pearson Correlation Coefficient - an overview | ScienceDirect Topics'. Accessed: Mar. 29, 2026. [Online]. Available: https://www.sciencedirect.com/topics/social-sciences/pearson-correlation-coefficient.
[95] Penalba M, Aizpurua JI, Martinez-Perurena A, Iglesias G. A data-driven long-term metocean data forecasting approach for the design of marine renewable energy systems. Renew Sustain Energy Rev Oct. 2022;167:112751. https://doi.org/10.1016/j.rser.2022.112751.
[96] Zhuang Y, Xu K, Bin L, Ma C, Zhang J, Lian J. Assessing China's wind-solar energy potential and complementarity under climate change: an environmental adaptability perspective. J Clean Prod Oct. 2025;528:146778. https://doi.org/10.1016/j.jclepro.2025.146778.
[97] G. N. Al Shabaan and I. S. Altarawneh, 'Decoding Climatic Drivers of Solar Photovoltaic Output in Arid Climates: Integrating Sensitivity, Lag Dynamics, and Principal Component Analysis for Forecasting Accuracy', *Sustain. Energy Technol. Assess.*, vol. 86, p. 104851, Feb. 2026, doi: 10.1016/j.seta.2026.104851.
[98] Yan BW, Li QS, Chan PW, He YC, Shu ZR. Characterising wind shear exponents in the offshore area using Lidar measurements. Appl Ocean Res Oct. 2022;127:103293. https://doi.org/10.1016/j.apor.2022.103293.
[99] L. Visser, E. Lorenz, D. Heinemann, and W. G. J. H. M. van Sark, '1.11 - Solar Power Forecasts', in *Comprehensive Renewable Energy (Second Edition)*, T. M. Letcher, Ed., Oxford: Elsevier, 2022, pp. 213–233. doi: 10.1016/B978-0-12-819727-1.00135-7.
[100] Deane JP, Drayton G, Gallachóir BPÓ. The impact of sub-hourly modelling in power systems with significant levels of renewable generation. Appl Energy Jan. 2014;113:152–8. https://doi.org/10.1016/j.apenergy.2013.07.027.
[101] Richardson D, Kilsby CG, Fowler HJ, Bárdossy A. Weekly to multi-month persistence in sets of daily weather patterns over Europe and the North Atlantic Ocean. Int J Climatol 2019;39(4):2041–56. https://doi.org/10.1002/joc.5932.
[102] Monforti F, Huld T, Bódis K, Vitali L, D'Isidoro M, Lacal-Arántegui R. Assessing complementarity of wind and solar resources for energy production in Italy. a Monte Carlo approach. Renew Energy Mar. 2014;63:576–86. https://doi.org/10.1016/j.renene.2013.10.028.